Article

Polyamine-dependent metabolic shielding regulates alternative splicing

https://doi.org/10.1038/s41586-025-09965-1

Received: 23 January 2024

Accepted: 26 November 2025

Published online: 14 January 2026

Open access

Check for updates

Amaia Zabala-Letona[1,2,27], Mikel Pujana-Vaquerizo[1,2,27], Belen Martinez-Laosa[1], Maria Ponce-Rodriguez[1], Saioa Garcia-Longarte[1,2], Isabel Mendizabal[1,3], Ana Gimeno[1,3], Malgorzata Rogalska[4], Joycelyn Tan[5], Diana Cabrera[1], Sebastiaan van Liempd[1], Pilar Ximenez-Embun[6], Sergio Espinosa[7,8,9], Maider Fagoaga-Eugui[1,2], Francesca Peccati[1,3], Maciej Zakrzewski[10], Ianire Astobiza[1,2], Mikel Arana-Castañares[1], Sarah Cherkaoui[11,12], Maria Sendino[13], Inés Martín-Barros[1], Amaia Ercilla[1,2,3], Laura Bozal-Basterra[1,2], Onintza Carlevaris[1], Amaia Arruabarrena-Aristorena[1,3,14], Encarnación Pérez-Andrés[1], Telmo Santamaría-Zamorano[1], Juan A. Ferrer-Bonsoms[15,16], Fernando Carazo[15,16], Maciej Cieśla[10], Cesar Lobato[15,16], Joan Seoane[2,9,17,18], Natalia Martín-Martín[1,2], Rosa Barrio[1], James D. Sutherland[1], Ana M. Aransay[1,19], Juan Manuel Falcón-Pérez[1,3,19], Barbara Martínez-Pastor[20], Angel Rubio[15,16], Francisco J. Blanco[1,3,21,22], Michael D. Hogarty[23,24], Raphael J. Morscher[11,12], Edurne Berra[1], Remigiusz A. Serwa[10], Jesús Jiménez-Barbero[1,3], Gonzalo Jiménez-Osés[1,3], Alejo Efeyan[20], Lydia Finley[5], Jose M. Lizcano[7,8], Javier Muñoz[3,6,13], Juan Valcarcel[4,17,25] & Arkaitz Carracedo[1,2,3,26] ✉

Metabolites are central to cellular homeostasis. Although much emphasis has been placed on their relevance to meet energetic and biosynthetic demands, metabolic intermediates also function as signalling molecules. Here we show that polyamines, small polycations that are critical to cellular homeostasis[1–3], regulate the process of alternative pre-mRNA splicing. We find that inhibition of polyamine synthesis increases phosphorylation of spliceosomal proteins, concomitant with perturbation of alternative splicing in cells and tissues. Mechanistically, molecular modelling combined with biochemical assays revealed that polyamines bind to acidic phosphorylatable motifs in splicing factors of the U2 small nuclear ribonucleoprotein SF3 subcomplex, thus preventing the action of upstream kinases. We refer to this molecular process by which polyamines regulate protein phosphorylation as metabolic shielding.

To identify molecular effectors of polyamines, we took advantage of a prostate cancer cell line (DU145) that exhibits strong sensitivity to inhibition of de novo polyamine biosynthesis[3], and we performed broad molecular characterization upon activation of an inducible short hairpin RNA (shRNA) targeting *S*-adenosylmethionine decarboxylase 1 (*AMD1*) (Supplementary Fig. 1a). Metabolic and proteic analyses revealed decreased AMD1 protein levels accompanied by a decrease in de novo synthesis of spermidine (Spd) and spermine (Spm) (by means of methionine-derived ^{13}C incorporation) at time points when the effect on total polyamine pools was less pronounced (Fig. 1a, Extended Data Fig. 1a and Supplementary Fig. 1b,c). We used isobaric labelling to measure abundances of peptides and phosphopeptides using mass spectrometry[4], and we found greater early perturbations in protein phosphorylation (Fig. 1b,c, Extended Data Fig. 1b,c and Supplementary Table 1). We performed a time-dependent trajectory analysis of phosphopeptide alterations (Fig. 1c) and focused on those showing the largest phosphoproteome changes (cluster 1), characterized by a progressive increase in phosphorylation over time. Functional enrichment

[1]Center for Cooperative Research in Biosciences (CIC bioGUNE), Basque Research and Technology Alliance (BRTA), Derio, Spain. [2]Centro de Investigación Biomédica En Red de Cáncer (CIBERONC), Madrid, Spain. [3]Ikerbasque Basque Foundation for Science, Bilbao, Spain. [4]Genome Biology Program, Centre for Genomic Regulation (CRG), The Barcelona Institute of Science and Technology, Barcelona, Spain. [5]Memorial Sloan Kettering Cancer Center (MSKCC), New York, NY, USA. [6]Proteomics Unit, Spanish National Cancer Research Centre (CNIO), Madrid, Spain. [7]Departament de Bioquímica i Biologia Molecular, Unitat de Medicina and Institut de Neurociències, Universitat Autònoma de Barcelona (UAB), Barcelona, Spain. [8]Protein Kinases in Cancer Research, Vall Hebron Institut de Recerca (VHIR), Barcelona, Spain. [9]Vall D´Hebron Instituto de Oncología (VHIO), Barcelona, Spain. [10]IMol Polish Academy of Sciences, Warsaw, Poland. [11]Pediatric Cancer Metabolism Laboratory, Children's Research Center, University of Zurich, Zurich, Switzerland. [12]Division of Oncology, University Children's Hospital Zurich and Children's Research Center, University of Zurich, Zurich, Switzerland. [13]Cell Signalling and Clinical Proteomics Group, Biobizkaia Health Research Institute, Barakaldo, Spain. [14]Department of Genetics, Physical Anthropology and Animal Physiology, University of the Basque Country UPV/EHU, Bilbao, Spain. [15]Departamento de Ingeniería Biomédica y Ciencias, TECNUN, Universidad de Navarra, San Sebastian, Spain. [16]Instituto de Ciencia de los Datos e Inteligencia Artificial (DATAI), Universidad de Navarra, Pamplona, Spain. [17]Institució Catalana de Recerca i Estudis Avançats (ICREA), Barcelona, Spain. [18]Universitat Autònoma de Barcelona, Barcelona, Spain. [19]Centro de Investigación Biomédica en Red de Enfermedades Hepáticas y Digestivas (CIBERehd), Madrid, Spain. [20]Metabolism and Cell Signalling Laboratory, Spanish National Cancer Research Center (CNIO), Madrid, Spain. [21]Instituto de Biomedicina de Valencia (IBV), Consejo Superior de Investigaciones Científicas, Valencia, Spain. [22]Centro de Investigación Príncipe Felipe (CIPF), Associated Unit to IBV, Valencia, Spain. [23]Division of Oncology and Department of Pediatrics, Children's Hospital of Philadelphia, Philadelphia, PA, USA. [24]Perelman School of Medicine at the University of Pennsylvania, Philadelphia, PA, USA. [25]Department of Medicine and Life Sciences, Universitat Pompeu Fabra (UPF), Barcelona, Spain. [26]Biochemistry and Molecular Biology Department, University of the Basque Country (UPV/EHU), Bilbao, Spain. [27]These authors contributed equally: Amaia Zabala-Letona, Mikel Pujana-Vaquerizo. ✉e-mail: acarracedo@cicbiogune.es

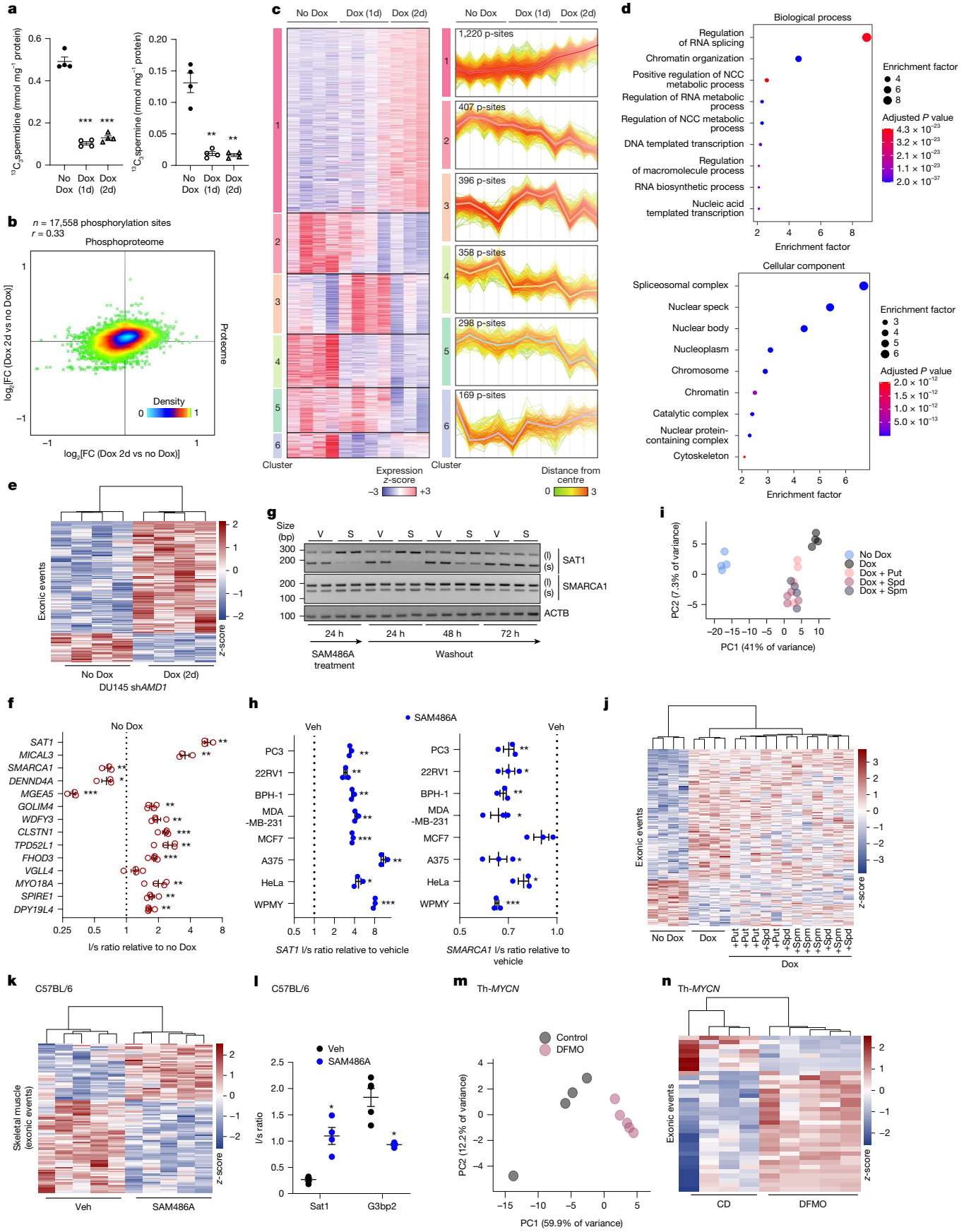

Fig. 1 | See next page for caption.

Fig. 1 | A phosphoproteomics-based discovery strategy reveals that inhibition of polyamine synthesis regulates the process of pre-mRNA splicing. a, Liquid chromatography–mass spectrometry (LC–MS) analysis of ^{13}C-labelled polyamine after inducible silencing of *AMD1* (for 1 day (1d) or 2 days (2d)) with doxycycline (Dox). $n = 4$ independent biological replicates. **b**, Bi-dimensional density plot showing the effect of *AMD1* silencing (2 days) on the phosphoproteome and the full proteome. FC, fold change. **c**, *z*-scored heat map of phosphorylation sites (p-sites) that are altered by *AMD1* silencing (compared with control (no Dox)) clustered by *k*-means. **d**, Gene ontology (GO) enrichment of phosphoproteins from cluster 1 in **c** by biological process and cellular component. NCC, nucleobase-containing compound. **e**, *z*-scored heat map of percent spliced in (PSI) alternative splicing events that are altered by *AMD1* silencing (sh*AMD1*; 2 days versus control (no Dox)) in DU145 cells (Abs(ΔPSI) > 10%, $P < 0.1$). **f**, Validation of top alternative splicing events, shown as fraction of long (l) versus short (s) transcripts (l/s ratio) from gel densitometry. $n = 3$ or 4 independent biological replicates. **g**, Semi-quantitative PCR showing the effect of SAM486A (0.5 μM, 24 h) on alternative splicing of *SAT1* and *SMARCA1* and recovery after drug washout (24–72 h). $n = 3$ independent biological replicates. S, SAM486A; V, vehicle. **h**, *SAT1* (left) and *SMARCA1* (right) l/s ratio after SAM486A (48 h) treatment of tumoural and non-tumoural cells by gel densitometry. $n = 3$ independent biological replicates. Veh, vehicle. **i**,**j**, Principal components analysis (**i**) and *z*-scored PSI heat map (**j**) (Abs(ΔPSI) > 10%, $P < 0.1$) of exonic events in DU145 cells treated with sh*AMD1* and induced with doxycycline (100 ng ml^{-1}) and supplemented with polyamines (10 μM, 2 days). **k**,**l**, *z*-scored PSI heat map of alternative splicing exonic events (**k**; $n = 5$ independent mice) and gel densitometry of *Sat1* and *G3bp2* l/s ratios (**l**; vehicle: $n = 5$, SAM486A: $n = 4$ independent mice) after SAM486A (8 days, 10 mg kg^{-1} day^{-1}) in skeletal muscle of wild-type mice (Abs(ΔPSI) > 10%, $P < 0.1$). **m**,**n**, Principal components analysis (**m**) and *z*-scored PSI heat map (**n**) of exonic events in Th-*Mycn* mice treated with DFMO ($n = 5$ independent mice) versus control ($n = 4$ independent mice). CD, control diet. One-tailed paired Student's *t*-test (**a**); one-tailed one-sample *t*-test (**f**); two-tailed one-sample *t*-test (**h**); two-tailed Mann–Whitney *U*-test (**l**). Adjusted *P* value was obtained by the multiple testing correction (set counts and sizes (SCS) method) (**d**). Data are mean ± s.e.m. ****$P < 0.0001$, ***$P < 0.001$, **$P < 0.01$, *$P < 0.05$; NS, not significant ($P \geq 0.05$).

analysis of this cluster revealed significant over-representation of proteins associated with the spliceosome, mRNA binding and regulation of mRNA splicing (Fig. 1d and Supplementary Fig. 1d).

Polyamines regulate alternative splicing

On the basis of these results, we explored whether polyamine biosynthesis regulates alternative splicing[5] using high-coverage RNA sequencing (RNA-seq). Estimation of alternative splicing using VAST-TOOLS[6] revealed remarkable changes in this process upon inhibition of polyamine biosynthesis (Fig. 1e, Extended Data Fig. 1d, Supplementary Fig. 1e and Supplementary Table 2). We identified robust events involving exon skipping (which included a gene encoding the polyamine homeostasis-regulating enzyme SAT1 (refs. 7–9)) and validated them by semiquantitative PCR with reverse transcription (RT–PCR) upon genetic silencing (*AMD1*, sh*AMD1*; *ODC1*, sh*ODC1*) or pharmacological inhibition (AMD1 inhibition with SAM486A; ODC1 inhibition with α-difluoromethylornithine (DFMO)) in a dose-dependent manner (note that the various perturbations exhibited different degrees of alternative splicing changes, possibly owing to the different temporal dynamics or the perturbation of different polyamine pools; Fig. 1f, Extended Data Fig. 1e–j and Supplementary Fig. 1f–h). The effects of polyamine synthesis inhibition by SAM486A on alternative splicing events were reversible upon inhibitor removal (Fig. 1g and Extended Data Fig. 1k), and were recapitulated in eight additional tumoural and non-tumoural cell lines (Fig. 1h, Extended Data Fig. 2a,b and Supplementary Fig. 1i).

To identify polyamine-regulated processes that could explain the alteration of alternative splicing, we first focused on their role in the regulation of cell cycle[3] and eIF5α hypusination[2]. We used cell cycle inhibitors (Supplementary Fig. 1j–n) or shRNA targeting of the hypusination machinery (deoxyhypusine synthase (*DHPS*) or *EIF5A1*; Supplementary Fig. 1o–q) and concluded that they did not mimic the changes in alternative splicing elicited by inhibitors of polyamine biosynthesis. Next, we studied the capacity of exogenous polyamines to revert the effects of polyamine biosynthesis inhibition and found that both individually and in combination, supplemented polyamines partially rescued the alteration in alternative splicing elicited upon *AMD1* silencing (Fig. 1i,j, Extended Data Fig. 2c,d, Supplementary Fig. 2a and Supplementary Table 3). In line with this notion, blocking ODC1 (using DFMO) in cells treated with SAM486A to further reduce polyamine levels (Extended Data Fig. 2e) potentiated the changes in alternative splicing (Extended Data Fig. 2f,g). Furthermore, supplementation with polyamines in cells treated with the combination of SAM486A and DFMO rescued the alterations in the phosphoproteome and alternative splicing (Extended Data Fig. 3a–f, Supplementary Fig. 2b,c and Supplementary Tables 4 and 5).

Next, we extended the observation of polyamine-regulated alternative splicing to in vivo experimental systems. First, we treated healthy adult male mice systemically with SAM486A and found that skeletal muscle, the tissue that showed the greatest impact on polyamine metabolism (by means of *S*-adenosylmethionine (dc-SAM) and Spm measurement) also presented robust changes in alternative splicing (Fig. 1k,l, Extended Data Fig. 3g–j, Supplementary Fig. 2d and Supplementary Table 6). Second, we confirmed alternative splicing changes in two clinically relevant neuroblastoma settings[10–12] treated with DFMO (Fig. 1m,n, Extended Data Fig. 3k–m, Supplementary Fig. 2e,f and Supplementary Tables 7 and 8). Overall, we conclude that inhibition of polyamine synthesis leads to robust alterations in alternative splicing in vitro and in vivo.

Spliceosome regulation by polyamines

To characterize the mechanism of polyamine-regulated splicing, we silenced *AMD1* in HeLa cells and, using RNA-seq, compared the alternative splicing profile to a systematic knockdown of more than 300 splicing factors and regulators[13–15]. In line with our previous observations, *AMD1* silencing elicited robust perturbation of alternative splicing, particularly affecting cassette exon skipping events (Fig. 2a, Extended Data Fig. 4a–c, Supplementary Fig. 3a,b and Supplementary Table 9). Remarkably, the extent of perturbation of alternative splicing upon *AMD1* silencing ranked in the top quartile of all splicing factor knockdowns analysed (Fig. 2b, Extended Data Fig. 4d and Supplementary Table 10). Jaccard similarity analysis revealed a strong resemblance between alternative splicing profiles elicited by inhibition of polyamine synthesis and silencing of different members of U2 small nuclear ribonucleoprotein (snRNP) SF3A and SF3B subcomplexes (SF3A and SF3B subunits) (Fig. 2c,d, Extended Data Fig. 4e, Supplementary Fig. 3c,d and Supplementary Table 10) that are involved in recognition of branch point sequences at the 3′ end of introns, subject to tight regulation through transcriptional and post-translational mechanisms and often altered in cancer[5,16–20].

The link between the activity of SF3 components and the effects of polyamine biosynthesis inhibition was also supported by the results of a complementary in silico approach, which leveraged available cross-linking immunoprecipitation with sequencing (CLIP–seq) datasets for multiple RNA-binding proteins[21,22] (Supplementary Methods). Components of the SF3 complex were significantly over-represented among the RNA-binding proteins that bind to transcripts that are alternatively spliced in DU145 cells upon *AMD1* knockdown (Figs. 1e, 2e, Extended Data Fig. 4f, Supplementary Fig. 3e and Supplementary Tables 11 and 12). To corroborate that the SF3 complex is relevant for polyamine-dependent regulation of alternative splicing, we inhibited

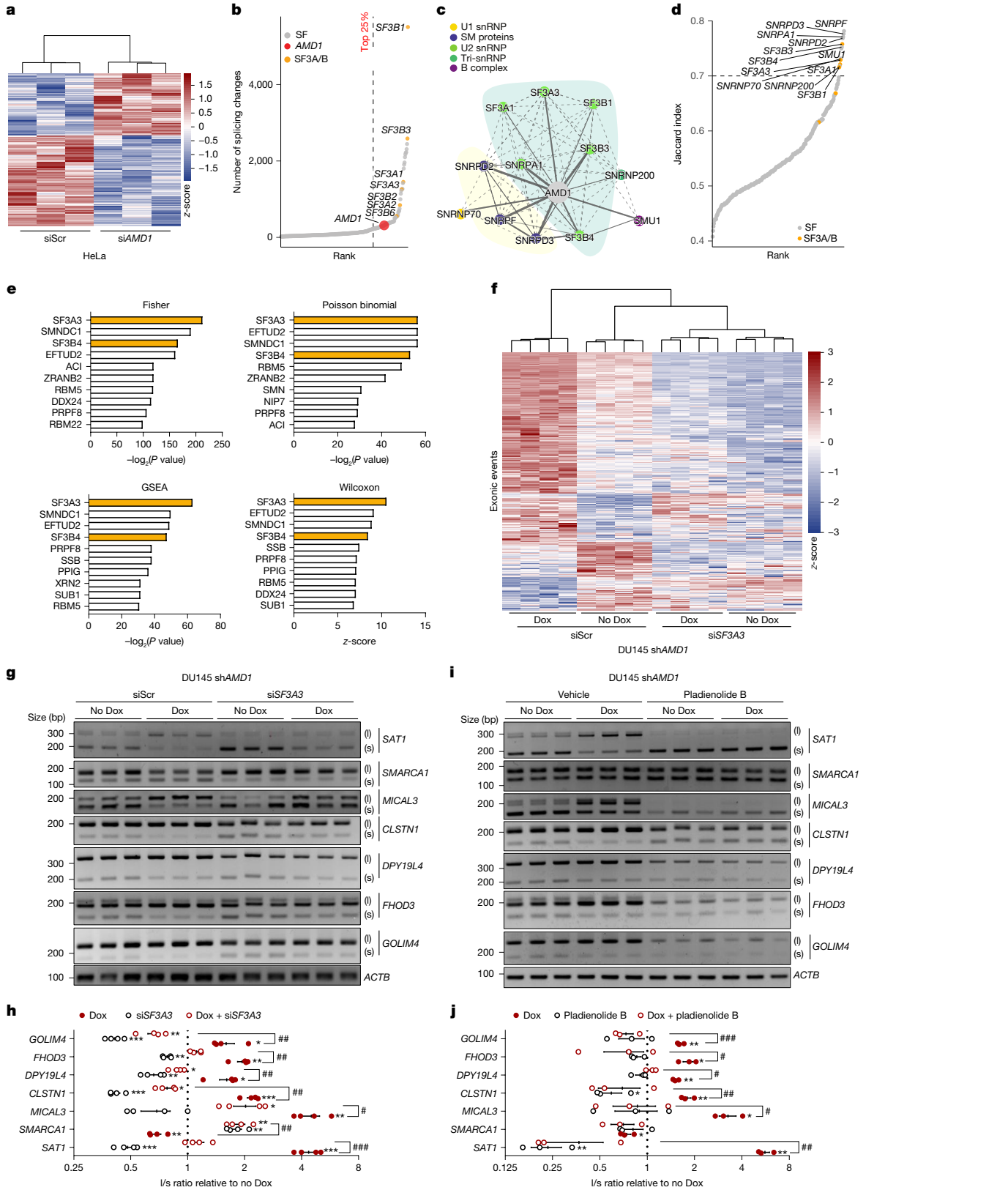

Fig. 2 | See next page for caption.

members of this complex using genetic (small interfering RNA (siRNA)) and pharmacological (pladienolide B, a SF3B complex inhibitor) means upon inhibition of polyamine biosynthesis (using sh*AMD1* or SAM486A). In agreement with our findings, interfering with the function of SF3 complex members abolished the consequences of polyamine biosynthesis inhibition for alternative splicing (Fig. 2f–j, Extended Data Fig. 4g–k, Supplementary Fig. 3f–j and Supplementary Table 13).

Next, we investigated whether biological processes that regulate polyamine biosynthesis could drive the observed changes in alternative

Fig. 2 | Regulation of alternative splicing upon polyamine deprivation requires the spliceosome U2 snRNP SF3 subcomplex. a, *z*-scored PSI heat map showing effects of *AMD1* silencing with small interfering RNA (si*AMD1*) on alternative splicing exonic events in HeLa cells (Abs(ΔPSI) > 10%, adjusted $P < 0.1$). siScr, scramble siRNA. **b**, Scatter plot of alternative splicing exonic events induced by silencing of *AMD1*, splicing factors (SF) or regulators (SF3A and SF3B complexes (SF3A/B)) in HeLa cells. **c**, Jaccard similarity plot and functional cloud showing proximity of AMD1 to splicing factors with overlapping splicing signatures in HeLa cells (exons). Solid edges indicate pairwise similarities, thickness represent Jaccard score and dashed edges show known protein–protein interactions in the spliceosome. Jaccard index cut-off = 0.7. **d**, Jaccard rank plot of shared exonic events resulting from silencing of *AMD1* and other genes encoding RNA-binding proteins. **e**, CLIP–seq based bar plots of splicing factors with mRNA binding sites and splicing perturbations consistent with *AMD1* silencing in DU145 cells, using EventPointer pipeline with Fisher, Poisson binomial, gene set enrichment analysis (GSEA) and Wilcoxon tests. U2 snRNP-associated proteins are highlighted in yellow. **f**, *z*-scored PSI heat map showing results of siRNA silencing of *SF3A3* (si*SF3A3*) in polyamine-high (no Dox) and polyamine-low (Dox) conditions. Only significant exonic events are shown (Abs(ΔPSI) > 10%, $P < 0.1$). **g**,**h**, Semi-quantitative PCR gels of long and short isoforms showing top exonic alternative splicing events upon *AMD1* shRNA silencing with or without si*SF3A3* in DU145 cells (**g**) and densitometry of l/s ratios versus controls (no Dox plus siScr) (**h**). $n = 4$ independent biological replicates. **i**,**j**, Semi-quantitative PCR gels showing long and short variants after *AMD1* shRNA silencing with or without the SF3B1 inhibitor pladienolide B (10 nM, 24 h) in DU145 cells (**i**), and densitometry of l/s ratios versus controls (**j**). $n = 3$ independent biological replicates. One-tailed one-sample *t*-test with 1 as hypothetical value (**h**,**j**). # indicates *P* values from one-tailed paired *t*-test for *SF3A3* silencing versus control under polyamine deprivation (**h**), or for pladienolide B versus control under polyamine deprivation (**j**). #$P < 0.05$, ##$P < 0.01$, ###$P < 0.001$. Data are mean ± s.e.m.

splicing and whether these effects were dependent on the integrity of the SF3 splicing complex. We found that hypoxia elicited: (1) a reduction in the expression of genes encoding polyamine biosynthetic enzymes (*ODC1*, *SRM* and *SMS*) in prostate cancer cells; (2) a global reduction in de novo polyamine biosynthesis (Extended Data Fig. 4l,m); and (3) a robust alteration in alternative splicing that was dependent on the SF3 complex (Extended Data Fig. 4n, Supplementary Fig. 4 and Supplementary Table 14).

Polyamines elicit metabolic shielding

Phosphorylation of spliceosome proteins is a well-established mechanism that is reported to regulate the splicing process[20,23]. We identified a series of phosphorylations in SF3 complex members in our original phosphoproteomics analysis that were preferentially assigned to cluster 1 in Fig. 1c (containing peptides which phosphorylation was increased upon *AMD1* silencing) (Fig. 3a). This cluster was characterized by peptides with a distinctively lower isoelectric point (Fig. 3b) and enrichment in the acidic amino acids aspartic acid and glutamic acid (Fig. 3c). Of note, supplementation with exogenous polyamines in cells with inhibition of de novo polyamine biosynthesis could revert the phosphorylation of the subset of upregulated peptides with low isoelectric point (Extended Data Fig. 5a,b), and we could confirm that the acidic phosphorylatable motifs of SF3 complex members were conserved and accessible for phosphorylation[24] (Extended Data Fig. 5c and Supplementary Fig. 5a). Given these results, we postulated that polyamines (owing to their cationic properties) interact with acidic phosphorylatable motifs in SF3 complex members, similar to previously reported interactions with other proteins[25,26]. These interactions would diminish accessibility of the phosphorylatable sites to upstream kinases (a phenomenon that we refer to as metabolic shielding) and reduce protein phosphorylation, thus influencing alternative splicing (see model in Extended Data Fig. 5d). Upon a reduction in polyamine levels, the phosphorylatable motifs would be exposed to upstream kinases, resulting in increased SF3 complex protein phosphorylation and alterations in alternative splicing. To validate this model, we first exploited molecular docking and molecular dynamics simulations to provide an atomistic, time-resolved representation of the interaction of putrescine (Put), Spd and Spm with the acidic phosphorylatable sites of a representative member of the SF3 subcomplex, namely SF3A3, whose acidic motif phosphorylation was reduced upon supplementation with polyamines (Extended Data Fig. 5e). As no complete, high-resolution structure is available for this protein, we generated full-atom AlphaFold models and docked Put, Spd and Spm on the phosphorylatable sites (Ser365, Ser367 and Ser369 in SF3A3). As predicted, the obtained binding poses (Fig. 3d and Supplementary Fig. 5b and Supplementary Fig. 6) revealed the formation of multiple salt bridges between the positively charged ammonium groups of polyamines and the negatively charged glutamic acid and aspartic acid residues flanking the phosphorylatable positions of SF3A3.

Using these docking poses as initial geometries, we performed molecular dynamics simulations to estimate the degree of shielding that each polyamine can provide to the various phosphorylatable positions. Such shielding exhibited fast statistical rebinding and was computed as the variation in the solvent-accessible surface area in the presence and absence of each polyamine[27] (Supplementary Table 15). The three polyamines showed distinct shielding capability at the phosphorylatable positions, roughly proportional to the number of ammonium groups, thereby enabling stronger interactions with clustered negatively charged residues. We analysed specific protein–ligand interactions between each polyamine and acidic residues surrounding the phosphorylatable serines (Supplementary Fig. 7a,b and Supplementary Table 16). All seven residues were engaged in transient salt bridge interactions, further confirming the electrostatic and statistical rebinding nature of polyamine binding (Supplementary Table 16). We utilized NMR to empirically test this model. We used the acidic phosphorylatable SF3A3 peptide (amino acids 350–380) as a proof of concept and determined its binding to polyamines. As a control, we used a phosphorylatable non-acidic peptide from SRRM1 (amino acids 374–406) that also presented three serines in proximity. The NMR analysis corroborated that Put, Spd and Spm interacted with the acidic phosphorylatable region of SF3A3 with 50–100 times greater affinity than SRRM1 and also presented an affinity towards this motif that was proportional to their cationic nature (in ascending order, Put < Spd < Spm) (Fig. 3e,f and Extended Data Fig. 6a–d). With these data, we computed the binding free energies of Put, Spd and Spm using umbrella sampling simulations towards both the full SF3A3 protein and the 350–380 model peptide used in the NMR analysis (Extended Data Fig. 6e). For the peptide, calculated binding energies were highly consistent with the NMR results (Supplementary Fig. 7c), thus validating the method. The interaction between the full SF3A3 protein and polyamines was calculated to be slightly stronger than with the peptide and in the low millimolar to high micromolar range. Also, in this case, binding free energy was more favourable for polyamines with more ammonium groups.

To corroborate the interaction between polyamines and SF3 complex members in cellulo, we took advantage of the recent implementation of photoaffinity labelling for polyamine research, which enabled us to monitor polyamine–protein interactions in cells[28]. HeLa cells were treated with a Spd probe bearing a minimal alkynyl diazirine photo-crosslinker or with vehicle control[29]. Following in-cell crosslinking, protein–probe conjugates were bioorthogonally ligated in cell lysates to azido derivatives of TAMRA or biotin (Extended Data Fig. 7a). SDS–PAGE with in-gel fluorescence scanning revealed the profile of probe-interacting proteins (Extended Data Fig. 7b), and

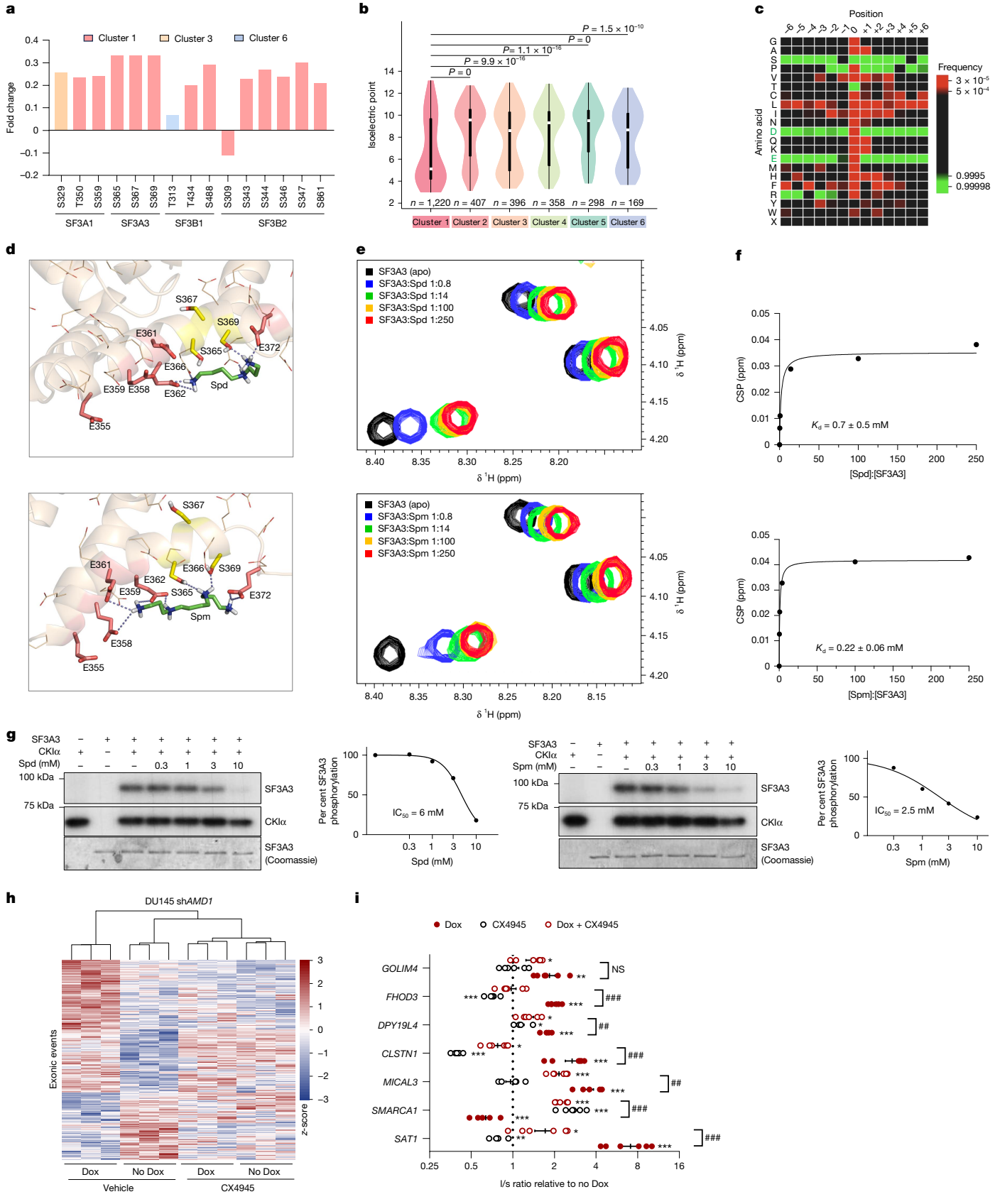

Fig. 3 | See next page for caption.

streptavidin-based enrichment and western blotting confirmed binding of the Spd probe to the SF3 subcomplex members SF3A3 and SF3B2 in cells (Extended Data Fig. 7c–f).

Our results support the notion that polyamine binding to acidic protein motifs could shield phosphorylatable residues from the action of kinases. We searched for kinases that were capable of phosphorylating

Fig. 3 | Polyamines bind acidic phosphorylatable motifs of splicing factors and prevent their phosphorylation. a, Bar plot of significantly altered phosphorylation sites ($P < 0.05$, FC ± 0.2) in U2 snRNP SF3 subcomplex members after inducible *AMD1* silencing (2 days, DU145 cells). **b**, Violin plot of isoelectric points of clusters that are altered upon polyamine deprivation by *AMD1* silencing in DU145 cells. White circles show medians, box limits indicate 25th and 75th percentiles, whiskers extend to 1.5 times the interquartile range from the 25th and 75th percentiles, and polygons represent density estimates of data and extend to extreme values. **c**, Heat map of amino acid abundance surrounding phosphorylation sites from cluster 1 after *AMD1* silencing (2 days, Dox versus no Dox). **d**, Representative binding modes for Spd (top) and Spm (bottom) on SF3A3. Spd and Spm are shown as green sticks, phosphorylatable residues (Ser365, Ser367, Ser369) are in yellow sticks and glutamic acid residues are shown as red sticks. **e**, Selected ^{1}H-^{1}H-total correlation spectroscopy (TOCSY) NMR spectra of SF3A3 fragment in without (black) or with (blue to red) increasing Spd (top) or Spm (bottom). Two spectra were omitted for clarity. **f**, Averaged chemical shift perturbation (CSP) from spectra in **e**, fitted to a 1:1 binding model with dissociation constant (K_d (± s.e.m.)). ppm, parts per million. **g**, Autoradiography showing ^{32}P incorporation into SF3A3 and CK1 after external addition of SF3A3 and CK1 with or without increasing Spd (left) or Spm (right). Kinetic titration: $n = 1$ independent biological replicate; reference concentration: $n = 2$ independent biological replicates. **h**, *z*-scored PSI heat map of alternative splicing exonic events altered by AMD1 silencing (2 days) with or without the CK2 inhibitor CX4945 (10 µM, 24 h) in DU145 cells (Abs(ΔPSI) > 10%, $P < 0.1$). **i**, I/s ratios for differential events in DU145 cells treated as in **h** determined by gel densitometry. $n = 6$ independent biological replicates. Two-tailed Mann–Whitney *U*-test (**b**); one-tailed one-sample *t*-test with 1 as hypothetical value (**i**). # indicates *P* values from one-tailed paired *t*-test for CX4945 versus control under polyamine deprivation. Data are mean ± s.e.m.

the selected sites. Using three different prediction algorithms, we identified CK1 and CK2 as frequently predicted upstream kinases for polyamine-regulated sites (Extended Data Fig. 7g). We selected CK1 for this assay to avoid the reported effect of polyamines on CK2 activity[25]. Next, we built a full-atom AlphaFold model of the SF3A3–CK1 complex in a putative catalytic state and docked the polyamines on the complex model using molecular dynamics (Extended Data Fig. 7h). Simulations revealed that polyamines adopt extended conformations to interact with both ATP phosphates and the negatively charged residues flanking the phosphorylatable positions, thus reducing phosphorylation activity towards SF3A3 (Extended Data Fig. 7h). Of note, the capacity of polyamines to prevent the recognition of the phosphorylatable motif by CK1 could not be assessed using this methodology but remains a plausible action of these metabolites. To confirm the capacity of polyamines to prevent the action of upstream kinases on SF3 complex members, we performed in vitro kinase assays. As predicted, CK1 phosphorylated recombinant SF3A3 (Fig. 3g). We performed a dose–response experiment with Spd and Spm to assess the concentrations of polyamines that could interfere with phosphorylation by CK1 (Fig. 3g) and confirmed this effect in independent biological replicates using 3 mM doses. In addition, all tested polyamines prevented the action of CK1-mediated phosphorylation on SF3A1 and SF3B2, with minimal interference in its autophosphorylation (Extended Data Fig. 7i,j).

Our data show that polyamines regulate the access of casein kinases to acidic phosphorylatable motifs in spliceosome components of the SF3 subcomplex. To assess the relevance of the process of phosphorylation in polyamine-regulated alternative splicing, we took advantage of CX4945, a pharmacological inhibitor of CK2 (ref. 30), which we found reduced the protein levels of CK1 in addition to its inhibitory action on its target, thus influencing the activity of the two major kinases predicted to target polyamine-regulated phosphorylation sites in the SF3 members (Extended Data Fig. 8a). We silenced *AMD1* in DU145 cells in the presence or absence of CX4945, and as predicted, CX4945 blunted the changes in alternative splicing elicited upon inhibition of polyamine synthesis (Fig. 3h,i, Extended Data Fig. 8b,c, Supplementary Fig. 8a and Supplementary Table 17). As a complementary strategy, we generated mice that were mutated in the three phosphorylation sites in the acidic motif of SF3A3 (S365, S367 and S369; *Sf3a3*$^{KI/KI}$ mice) using CRISPR–Cas9-based gene editing and collected mouse embryonic fibroblasts (MEFs) for molecular analysis (Extended Data Fig. 8d,e). Wild-type and homozygous mutant MEFs responded similarly to SAM486A in terms of polyamine biosynthesis (Extended Data Fig. 8f). Of note, *Sf3a3*$^{KI/KI}$ MEFs presented basal changes in alternative splicing compared with wild-type counterparts, with 312 differential events (112 events assigned to exon skipping; ΔPSI > 10% and a Wilcoxon *P* value < 0.1). We then focused on alternative splicing events perturbed by polyamine biosynthesis inhibition in wild-type MEFs. When challenged with AMD1 inhibitor, we observed 260 differentially spliced events, whereas 96% of these remained unaltered in *Sf3a3*$^{KI/KI}$ mutant cells (only 10 out of 260 events exhibited a ΔPSI greater than 10% and a Wilcoxon *P* value < 0.1), suggesting that phosphorylation of S365, S367 and S369 in SF3A3 is relevant, at least partly, for the regulation of alternative splicing and upon inhibition of polyamine biosynthesis (Extended Data Fig. 8g, Supplementary Fig. 8b and Supplementary Table 18).

We aimed to determine whether the acidic amino acids in the phosphorylatable region of SF3A3 were required for the effect of polyamines on alternative splicing. To achieve this, we modelled and produced a SF3A3 peptide (amino acids 350–380) with mutations in all glutamic acid and aspartic acid residues in this region. However, the mutant protein was unstable, showed no ability to bind polyamines according to molecular dynamics simulations (Supplementary Fig. 9a–c) and precipitated in the process of purification, which prevented us from performing further empiric analyses. As an alternative approach, we sought to identify specific acidic amino acids that, when mutated, would reduce the metabolic shielding effect of polyamines without influencing overall stability of the protein. Using AlphaFold 3.0 to model the molecular interactions between SF3A3 and CK1, we selected three regions with acidic residues through which polyamines could disrupt the interaction with the kinase (Supplementary Fig. 10a) and mutated them to their neutral equivalents (asparagine and glutamine) (Supplementary Fig. 10b). We estimated the relevance of polyamine-based shielding in these regions by calculating the Rosetta energy units for the SF3A3–CK1 interaction and found that variant 3 would be predicted to exert the strongest perturbation (Supplementary Fig. 10b). We combined SF3A3 silencing with the overexpression of shRNA-resistant forms of wild-type and mutant SF3A3 in DU145 cells and could only detect some degree of loss of responsiveness to polyamine depletion-elicited changes in alternative splicing of variant 3 (in line with the computational estimations; Supplementary Fig. 10c–e). There are two important aspects that should be considered. First, although we predict that these mutant proteins would have weakened polyamine binding, the amino acid changes could also influence the recognition by the kinase, thus making any experimental interpretation of the results challenging. Second, since various SF3 subcomplex members are subject to metabolic shielding, altering the phosphorylation or shielding capacity of a single member would be insufficient to fully abolish the consequences of the inhibitors of polyamine biosynthesis on alternative splicing.

BENSpm shows metabolic shielding ability

Our results suggest that metabolic shielding could explain molecular and biological actions of polyamines that are distinct from their conventional activities. Based on the proposed mechanism of action of metabolic shielding, we postulated that strongly cationic polyamine-like molecules could replicate this phenomenon and serve as discovery platforms for processes regulated by this mechanism. We took advantage of N^1,N^{11}-bis(ethyl)norspermine (BENSpm), an Spm analogue that strongly

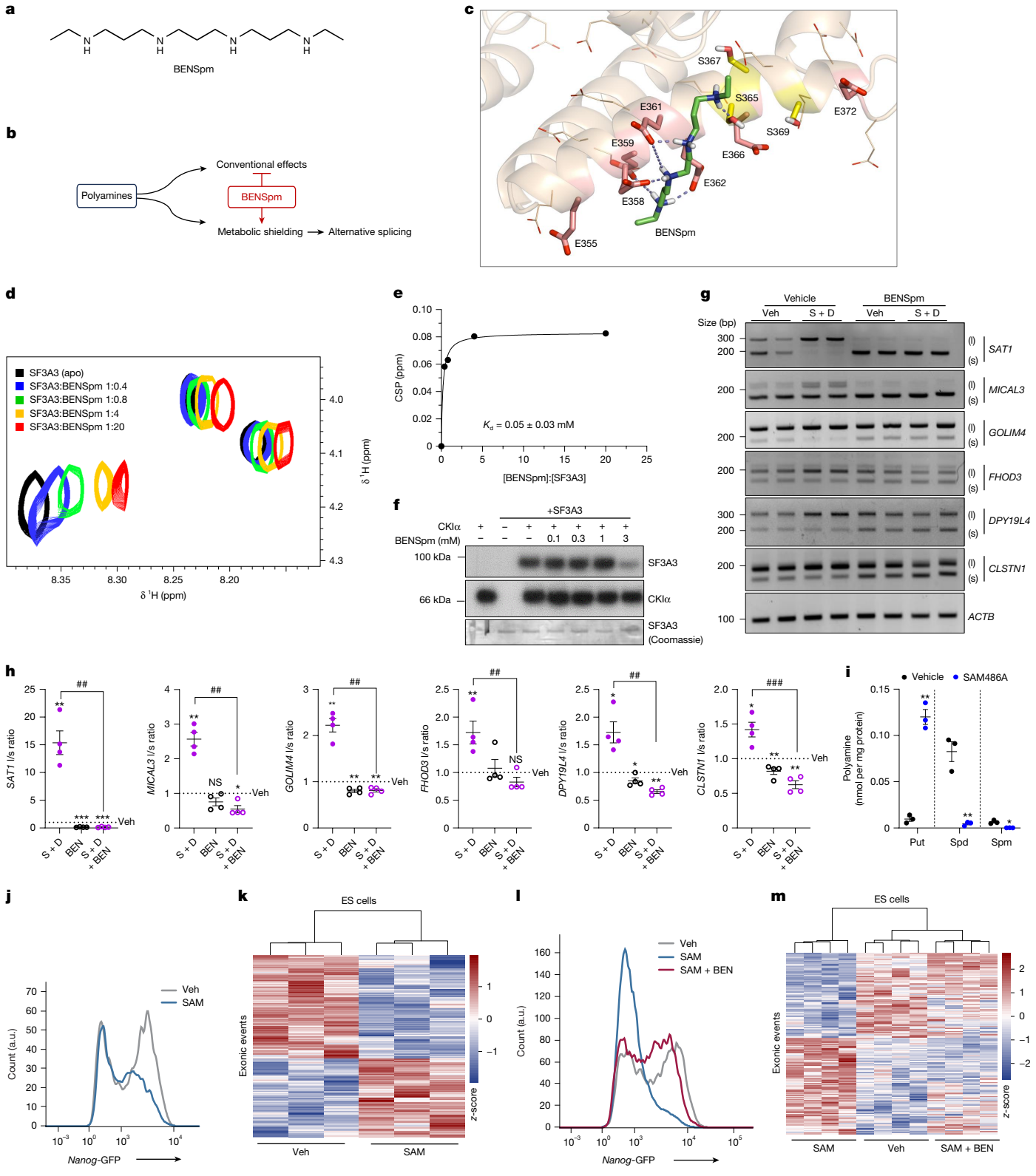

Fig. 4 | See next page for caption.

inhibits polyamine biosynthesis but retains a polyamine-like cationic nature[31] (Fig. 4a). We reasoned that BENSpm, by reducing polyamine levels, would inhibit conventional molecular and biological responses of this metabolic pathway. By contrast, as it retains a strong polycationic nature, BENSpm would rescue the lack of endogenous polyamines in processes regulated by metabolic shielding (Fig. 4b). As predicted, BENSpm interacted with the acidic region of SF3A3, as measured using molecular dynamics and NMR (Fig. 4c–e, Extended Data Fig. 9a–d and Supplementary Tables 19 and 20), and prevented the action of CK1 on this phosphorylatable region (Fig. 4f and Extended Data Fig. 9c). Notably, incubation with BENSpm prevented the changes in alternative splicing elicited upon treatment with SAM486A plus DFMO, despite the profound inhibition of de novo polyamine biosynthesis (Fig. 4g,h and Extended Data Fig. 9e).

Fig. 4 | BENSpm elicits metabolic shielding and prevents polyamine depletion-triggered ES cell differentiation. a, Schematic of the BENSpm molecule. **b**, Mechanism of action of BENSpm: antagonizing natural polyamine functions while mimicking metabolic shielding owing to its cationic nature. **c**, Representative binding mode of BENSpm on SF3A3. BENSpm is shown as green sticks, phosphorylatable residues (Ser365, Ser367 and Ser369) are in yellow and glutamic acid residues are in red. **d**, Selected ^{1}H-1H-TOCSY NMR spectra of the SF3A3 fragment without (black) or with increasing BENSpm (blue to red). **e**, Average chemical shift perturbations from spectra in **d**, fitted to a 1:1 binding model with dissociation constant (s.e.m.). **f**, Autoradiography showing ^{32}P incorporation into SF3A3 and CK1 after addition of SF3A3 and CK1 with or without BENSpm. $n = 3$. **g**,**h**, Semi-quantitative PCR gels (**g**) and densitometry (**h**) showing l/s ratios after BENSpm (10 μM, 48 h (BEN)) treatment in vehicle conditions and with AMD1 and ODC1 inhibition (SAM486A 1 μM + DFMO 50 μM, 48 h (S + D)) for validated alternative splicing candidates. $n = 4$ **i**–**k**, Polyamine quantification by LC–MS (**i**; $n = 3$), *Nanog*-GFP expression by flow cytometry (**j**; $n = 2$) and *z*-scored PSI heat map of alternative splicing events (**k**) in mouse ES cells transduced with *Nanog*-GFP and treated with SAM486A (0.5 μM, 48 h). **l**,**m**, *Nanog*-GFP flow cytometry (**l**; $n = 2$) and RNA-seq (shown as *z*-scored PSI heat map, **m**) of ES cells with *Nanog*-GFP treated with or without SAM486A (0.5 μM, 48 h) and BENSpm (10 μM, 48 h). One-tailed one-sample *t*-test with 1 as hypothetical value (**h**); two-tailed paired Student's *t*-test for metabolomics (**i**). # indicates *P* values from two-tailed paired *t*-test for S + D versus S + D + BENSpm. Data are mean ± s.e.m.

Metabolic shielding controls ES cell function

We next tested whether BENSpm could be a useful tool for distinguishing biological consequences of polyamine deprivation that emanate from conventional functions versus metabolic shielding. Spm supplementation in cells treated with polyamine synthesis inhibitors rescued the cell proliferation defect. By contrast, BENSpm did not exert such rescue, and it induced a reduction in cell growth as single agent, in line with its capacity to inhibit polyamine production in cancer cells[31] (Extended Data Fig. 9f–i). Next, we searched for biological functions of polyamines beyond cancer and cell proliferation and focused on their reported requirement for embryonic stem (ES) cell self-renewal[32]. Using ES cells expressing a reporter of *Nanog* expression, we corroborated that inhibition of de novo polyamine synthesis resulted in loss of *Nanog*-GFP expression (a surrogate for pluripotent self-renewal) (Fig. 4i,j and Extended Data Fig. 10a–d) and elicited a change in the alternative splicing landscape (Fig. 4k, Extended Data Fig. 10e–h and Supplementary Tables 21 and 22). We then treated polyamine-deprived ES cells with BENSpm and evaluated the effect on *Nanog* expression and alternative splicing. Of note, BENSpm reverted the effects of SAM486A or DFMO on pluripotent self-renewal (based on the proportion of *Nanog*-GFP-positive cells) and alternative splicing (Fig. 4l,m, Extended Data Fig. 10i–r and Supplementary Tables 23 and 24). Our data reveal that ES cell maintenance requires polyamine production to sustain the stemness properties, through a mechanism that involves, at least in part, metabolic shielding.

Discussion

Our findings uncover a new mode of action of polyamines, according to which their cationic nature mediates the interaction with phosphorylatable acidic motifs and prevents the action of kinases. We attribute polyamine-regulated alternative splicing to the process of metabolic shielding. Molecular dynamics and NMR analyses revealed that the metabolic shielding capacity of polyamines is dependent on their cationic nature. Of note, our findings on protein phosphorylation could theoretically be expanded to other post-translational modifications located in acidic motifs.

The metabolic shielding effect is more closely associated with the timing of perturbation of de novo polyamine production than the total polyamine pools. A substantial fraction of polyamines is accumulated in polyamine-sequestering vesicles[33] and is therefore potentially biologically inactive. Thus, de novo-produced polyamines might more closely reflect the biologically active metabolite fraction that regulates the process of metabolic shielding. With the improvements in metabolite detection and quantification, we may begin to isolate the compartmentalized production and accumulation of polyamines, which will propel our understanding of the biological and molecular repercussions of metabolic shielding. In addition, the use of polycationic molecules such as BENSpm (a polyamine analogue that inhibits the production of these metabolites and mimics their metabolic shielding activity) will help in classifying polyamine-regulated processes into conventional versus metabolic shielding, and thus advance comprehension of the mechanistic bases of polyamine function in health and disease.

Online content

Any methods, additional references, Nature Portfolio reporting summaries, source data, extended data, supplementary information, acknowledgements, peer review information; details of author contributions and competing interests; and statements of data and code availability are available at https://doi.org/10.1038/s41586-025-09965-1.

1. Holbert, C. E., Cullen, M. T., Casero, R. A. Jr & Stewart, T. M. Polyamines in cancer: integrating organismal metabolism and antitumour immunity. *Nat. Rev. Cancer* **22**, 467–480 (2022).
2. Arruabarrena-Aristorena, A., Zabala-Letona, A. & Carracedo, A. Oil for the cancer engine: the cross-talk between oncogenic signaling and polyamine metabolism. *Sci. Adv.* **4**, eaar2606 (2018).
3. Zabala-Letona, A. et al. mTORC1-dependent AMD1 regulation sustains polyamine metabolism in prostate cancer. *Nature* **547**, 109–113 (2017).
4. Martinez-Val, A. et al. Dissection of two routes to naïve pluripotency using different kinase inhibitors. *Nat. Commun.* **12**, 1863 (2021).
5. Rogalska, M. E., Vivori, C. & Valcárcel, J. Regulation of pre-mRNA splicing: roles in physiology and disease, and therapeutic prospects. *Nat. Rev. Genet.* **24**, 251–269 (2023).
6. Gohr, A. et al. Computational analysis of alternative splicing using VAST-TOOLS and the VastDB framework. *Methods Mol. Biol.* **2537**, 97–128 (2022).
7. Hyvonen, M. T. et al. Polyamine-regulated unproductive splicing and translation of spermidine/spermine N1-acetyltransferase. *RNA* **12**, 1569–1582 (2006).
8. Hyvonen, M. T. et al. Tissue-specific alternative splicing of spermidine/spermine N1-acetyltransferase. *Amino Acids* **42**, 485–493 (2012).
9. Yang, Q. et al. Knockdown of SSATX, an alternative splicing variant of the SAT1 gene, promotes melanoma progression. *Gene* **716**, 144010 (2019).
10. Yang, J. Approval of DFMO for high-risk neuroblastoma patients demonstrates a step of success to target MYC pathway. *Br. J. Cancer* **130**, 513–516 (2024).
11. Weiss, W. A., Aldape, K., Mohapatra, G., Feuerstein, B. G. & Bishop, J. M. Targeted expression of MYCN causes neuroblastoma in transgenic mice. *EMBO J.* **16**, 2985–2995 (1997).
12. Cherkaoui, S. et al. Reprogramming neuroblastoma by diet-enhanced polyamine depletion. *Nature* **646**, 707–715 (2025).
13. Papasaikas, P., Tejedor, J. R., Vigevani, L. & Valcárcel, J. Functional splicing network reveals extensive regulatory potential of the core spliceosomal machinery. *Mol. Cell* **57**, 7–22 (2015).
14. Tejedor, J. R., Papasaikas, P. & Valcárcel, J. Genome-wide identification of Fas/CD95 alternative splicing regulators reveals links with iron homeostasis. *Mol. Cell* **57**, 23–38 (2015).
15. Carbonell, C. et al. Functional network analysis reveals the relevance of SKIIP in the regulation of alternative splicing by p38 SAPK. *Cell Rep.* **27**, 847–859.e846 (2019).
16. Wahl, M. C., Will, C. L. & Lührmann, R. The spliceosome: design principles of a dynamic RNP machine. *Cell* **136**, 701–718 (2009).
17. Cieśla, M. et al. Oncogenic translation directs spliceosome dynamics revealing an integral role for SF3A3 in breast cancer. *Mol. Cell* **81**, 1453–1468.e1412 (2021).
18. Yoshida, K. et al. Frequent pathway mutations of splicing machinery in myelodysplasia. *Nature* **478**, 64–69 (2011).
19. Liu, Z. et al. Pan-cancer analysis identifies mutations in SUGP1 that recapitulate mutant SF3B1 splicing dysregulation. *Proc. Natl Acad. Sci. USA* **117**, 10305–10312 (2020).
20. Hluchý, M. et al. CDK11 regulates pre-mRNA splicing by phosphorylation of SF3B1. *Nature* **609**, 829–834 (2022).
21. Ferrer-Bonsoms, J. A. et al. EventPointer 3.0: flexible and accurate splicing analysis that includes studying the differential usage of protein-domains. *NAR Genomics Bioinformatics* **4**, lqac067 (2022).
22. Lobato-Fernandez, C., Gimeno, M., San Martín, A., Anorbe, A., Rubio, A. & Ferrer-Bonsoms, J. A. A systematic identification of RNA-binding proteins (RBPs) driving aberrant splicing in cancer. *Biomedicines* **12**, 2592 (2024).
23. Cao, W., Jamison, S. F. & Garcia-Blanco, M. A. Both phosphorylation and dephosphorylation of ASF/SF2 are required for pre-mRNA splicing in vitro. *RNA* **3**, 1456–1467 (1997).
24. Zhan, X., Yan, C., Zhang, X., Lei, J. & Shi, Y. Structures of the human pre-catalytic spliceosome and its precursor spliceosome. *Cell Res.* **28**, 1129–1140 (2018).

25. Leroy, D., Heriché, J. K., Filhol, O., Chambaz, E. M. & Cochet, C. Binding of polyamines to an autonomous domain of the regulatory subunit of protein kinase CK2 induces a conformational change in the holoenzyme. A proposed role for the kinase stimulation. *J. Biol. Chem.* **272**, 20820–20827 (1997).
26. Lefèvre, J. et al. The C terminus of tubulin, a versatile partner for cationic molecules: binding of Tau, polyamines, and calcium. *J. Biol. Chem.* **286**, 3065–3078 (2011).
27. Richmond, T. J. Solvent accessible surface area and excluded volume in proteins. Analytical equations for overlapping spheres and implications for the hydrophobic effect. *J. Mol. Biol.* **178**, 63–89 (1984).
28. Zakrzewski, M. et al. Profiling polyamine–protein interactions in live cells through photoaffinity labeling. *RSC Chem. Biol.* **6**, 1787–1796 (2025).
29. Pan, S. et al. A suite of "minimalist" photo-crosslinkers for live-cell imaging and chemical proteomics: case study with BRD4 inhibitors. *Angew. Chem. Int. Ed.* **56**, 11816–11821 (2017).
30. Siddiqui-Jain, A. et al. CX-4945, an orally bioavailable selective inhibitor of protein kinase CK2, inhibits prosurvival and angiogenic signaling and exhibits antitumor efficacy. *Cancer Res.* **70**, 10288–10298 (2010).
31. Gabrielson, E. W., Pegg, A. E. & Casero, R. A. Jr. The induction of spermidine/spermine N1-acetyltransferase (SSAT) is a common event in the response of human primary non-small cell lung carcinomas to exposure to the new antitumor polyamine analogue N^1,N^{11}-bis(ethyl)norspermine. *Clin. Cancer Res.* **5**, 1638–1641 (1999).
32. Zhang, D. et al. AMD1 is essential for ESC self-renewal and is translationally down-regulated on differentiation to neural precursor cells. *Genes Dev.* **26**, 461–473 (2012).
33. Holbert, C. E., Casero, R. A. Jr & Stewart, T. M. Polyamines: the pivotal amines in influencing the tumor microenvironment. *Discov. Oncol.* **15**, 173 (2024).

Methods

Animals

Experimental procedures involving the use of mice were carried out following the ethical guidelines established by the Biosafety and Animal Welfare Committee at CICbioGUNE, under ethics protocol P-CBG-CBBA-0121. The procedures were performed in concordance with the recommendations stablished by the AAALAC. Mice on a mixed background were housed under controlled environmental conditions, such as time-controlled lighting on standard 12 h:12 h light:dark cycles, controlled temperature at 22 ± 2 °C and 30–50% relative humidity. Mice were fed regular chow diet ad libitum and fasted for 6 h prior to tissue collection (09:00–15:00) to prevent metabolic alterations due to immediate food intake. At the experimental end-point, all mice were euthanized by CO_2 inhalation followed by cervical dislocation.

Sf3a3$^{KI/KI}$ mouse generation

To engineer *Sf3a3*$^{KI/KI}$ mice, zygotes were obtained from crosses between C57Bl6 male mice and hybrid C57Bl6.CBA female mice. Zygotes were injected with Cas9 and a guide RNA (gRNA) (Cr/Trac) targeting the sequence of interest and a repair single-stranded oligonucleotide containing the intended mutations flanked by 80 bp of homology arms adjacent to the double-strand break site. Genotyping was performed by specific amplification followed by Sanger sequencing. The single guide RNA (sgRNA) used was GATCAGCGA GAGCGAAAGTGAGG and the repair single-stranded oligonucleotide was GAACAGCGACAGCTCACTCATGAAAATGTTCAGCGCAAGCAAGCC AGGACAGGCGAGGAGCGGGAGGAGGAGGAGGAGGAGCAGATCGCCGA GGCAGAAGCTGAAGACGAAGAGAATGAGATCATTTACAACCCCAAGAA CCTGCCGCTGGGCTGGGACGGCAAGGTAAGGTCTCAGGGCCCTCTGT CCCCTTCCATCATGGGCATGCCTGAGCTCGGAAATCTCATGCAGTCGC TTTCCTTTAGCCCATCCCCTACTGGCTGTAC. All CRISPR reagents were purchased from Integrated DNA Technologies. gRNA was assembled from Alt-R CRISPR–Cas9 CRISPR RNA (crRNA; 5′-GATCAGCGAG AGCGAAAGTG-3′) and Alt-R CRISPR–Cas9 *trans*-activating crRNA (tracrRNA) in microinjection buffer (10 mM Tris/HCl pH 7,5; 0.1 mM EDTA) by heating for 5 min at 95 °C in a thermocycler and decreasing temperature slowly using a pre-defined temperature ramp. Assembled tracrRNA and crRNA gRNAS were incubated with Alt-R *Sp*Cas9 Nuclease V3 to form the ribonucleoprotein complex for 15 min at room temperature in microinjection buffer and injected at a final concentration of 1.2 μM and 0.24 μM, respectively. Donor oligodeoxynucleotide was added at a final concentration of 10 ng μl^{-1}.

CRISPR reagents (Integrated DNA Technologies) were microinjected in the pronucleus of zygotes obtained from crosses between C57Bl6 males and hybrid B6.CBA female mice. Female mice (5–8 weeks of age) were previously superovulated by consecutive administration of 5 IU of pregnant mare serum gonadotropin (PMSG) (at 15:00 of day −3) and 5 IU of human chorionic gonadotropin (hCG) (at 13:00 of day −1), and matings were set up immediately after hCG administration. At 8 pm of day 0, the formation of vaginal plugs was monitored and cumuli were collected from oviducts. Cumuli were disaggregated with a hyaluronidase (Sigma H4272) solution (10 mg ml^{-1} in M2 medium) diluted 1:2 in M2 medium at the moment of treatment. Free zygotes were cultured in KSOM medium until injection. On the next day, zygotes that had developed to the 2-cell stage were transferred to pseudopregnant CD1 female mice according to standard protocols[34].

Reagents

The human prostate carcinoma cell lines used were purchased from Leibniz-Institut DSMZ (Deutsche SammLung von Mikroorganismen und Zellkulturen GmbH), which provided authentication certificates: DU145 (ACC261), PC3 (ACC465), 22RV1 (ACC438) and human benign prostatic hyperplasia (BPH-1) (ACC143). WPMY-1 prostate stroma fibroblast cell line was purchased from ATCC (CRL-2854). Virus packaging cell line (HEK 293FT; Invitrogen) was provided by R. Barrio and J. Sutherland. Human breast cancer cell lines were purchased from DMSZ: MCF7 (ACC115) and MDA-MB-231 (ACC732). Human melanoma cell line A375 was purchased from ATCC (CRL-1619). J. Valcarcel provided the HeLa cervical carcinoma cell line. SKNBE2 cell line were provided by the Children's Oncology Group Cell Culture Repository (https://cccells.org) with authentication certificates. In all the cases cells tested negative for mycoplasma. DFMO (prepared in water, final concentration 25–500 μM), doxycycline (prepared in water, final concentration 0.1–0.15 μg ml^{-1}), pladienolide B (prepared in DMSO, final concentration 10 nM), Spd (prepared in water, final concentration 0.3–10 mM for kinase assay and 10 μM for other assays), Spm (prepared in water, final concentration 0.3–10 mM for kinase assay and 10 μM for other assays), Put (prepared in water, final concentration 0.3–30 mM for kinase assay and 10 μM for other assays), BENSpm (prepared in water, final concentration 0.3–3 mM for kinase assay and 10 μM for other assays), synthetic Spd photoaffinity probe (prepared in water, final concentration 5 μM), aminoguanidine (prepared in water, final concentration 1 mM), SAM486A (prepared in water, final concentration 0.1–5 μM in vitro, 10 mg per kg (body weight) per day intraperitoneally for 8 days, in vivo), thymidine (prepared in water, final concentration 2 mM), CX4945 (prepared in DMSO, final concentration 10 μM) were obtained from Sigma-Aldrich (doxycycline, thymidine, aminoguanidine, Spd, Spm and Put), SCBT (pladienolide B), Tocris (DFMO and N^1,N^{11}-diethylnorspermine) and LabNet Biotecnica (CX4945), and SAM486A was provided by Novartis. [U-$^{13}C_5$] L-methionine was purchased from Cambridge Isotope Laboratories and dosed at a final concentration of 30 μg ml^{-1} in vitro. Doxycycline was used at 100 ng ml^{-1} for silencing of *AMD1*, and 150 ng ml^{-1} for silencing of *ODC1*, *DHPS* and *EIF5A1*. shRNA targeting *AMD1* was purchased from Sigma (TRCN0000078460) and described elsewhere[3]. shRNA targeting *ODC1*, *DHPS* and *EIF5A1* were purchased from Sigma (TRCN0000333342, TRCN0000045644 and TRCN0000062548, respectively). The control shRNA sequence was CCGGCAACAAGATGAAGAGCACCAACTC |GAGTTGGTGCTCTTCATCTTGTTG[35]. Sub-cloning of sh*ODC1*, sh*DHPS* and sh*EIF5A1* into pLKO-Tet-On vector were done introducing AgeI and EcoRI in the 5′ end of top and bottom shRNA oligonucleotides, respectively (TET-pLKO puro was a gift from D. Wiederschain[36] (Addgene plasmid #21915)). Lentiviral transductions were performed as previously described[3]. siRNAs for transient transfections were purchased from Dharmacon and used at a final concentration of 25 nM (siScr: D-001810-10-05, si*AMD1*; L-010053-01-0005, si*SF3A1*; L-016051-00-0005, si*SF3A3*; L-019808-00-0005, si*SF3B1*; L-020061-01-0005).

Cellular and molecular assays

Cell number quantification for growth curve and focus assays was done with crystal violet[3]. DU145 cells submitted to hypoxic conditions were incubated in hypoxia incubator (Baker) at 1% hypoxia for 24 h. Polyamine supplementation experiments were complemented with 1 mM aminoguanidine to avoid polyamine oxidation in media. Western blot was performed as previously described[3], run in NUPAGE gradient precast gels (Life Technologies) in MOPS buffer. Primary antibodies were used at 1:1,000. Anti-AMD1 (11052-1-AP, Proteintech); anti-ODC1 (17003-1-AP, Proteintech); anti-PAOX (18972-1-AP, Proteintech); anti-SAT1 (10708-1-AP, Proteintech); anti-SMOX (15052-1-AP, Proteintech); anti-CK1 (2655, CST) and anti-HSP90 (4874S, CST). Secondary anti-rabbit antibody was used at 1:4,000 and purchased from Jackson ImmunoResearch. RNA was extracted using NucleoSpin RNA isolation kit from Macherey-Nagel (ref: 740955.240 C) or automatically extracted using Maxwell RSC instrument (Promega) according to the manufacturers' instructions (Supplementary Methods).

RNA-seq analysis

The quantity and quality of RNA were evaluated using Qubit RNA HS Assay Kit (Thermo Fisher Scientific, Q32855) and Agilent RNA 6000 Nano Chips (Agilent Technologies, 5067-1511), respectively.

mRNA sequencing libraries were generated following *TruSeq Stranded mRNA Sample Preparation Guide* (15031058 rev. E) using the TruSeq Stranded mRNA Library Prep kit (Illumina, 20020594) and TruSeq RNA CD Index Plate (96 indexes, 96 samples) (Illumina, 20019792) except for the following cases. For the CK2 inhibitor (CX4945) experiment in DU145 cells, mRNA libraries were prepared using Illumina Stranded mRNA Prep kit (Illumina, 20040532), following *Illumina Stranded mRNA Prep Reference Guide* (1000000124518 v.02). For hypoxia RNA seq analysis in DU145 cells, total RNA libraries were prepared using the TruSeq Stranded Total RNA with Ribo-Zero kit (Illumina 20020612) and TruSeq RNA CD Index Plate (Illumina 20019792) following *TruSeq Stranded Total RNA Sample Prep-Guide* (15031048 rev. E).

After a final library clean-up, all libraries were reviewed on an Agilent 2100 Bioanalyzer using Agilent High Sensitivity DNA kits (Agilent Technologies, 5067-4626) and quantified using Qubit dsDNA HS DNA Kit (Thermo Fisher Scientific, Q32854).

Sequencing was performed on an Illumina NovaSeq 6000 system. A paired-end type of read with a length of 150 bp was performed unless otherwise specified.

RNA-seq of si*AMD1* versus siScr samples was performed in the Centre for Genomic Regulation (CRG). Stranded mRNA-seq libraries were prepared and two samples/lane were sequenced, following 2× 125 nt paired-end protocol at the CRG Genomics Core Facility on a HiSeq 2500 v.4 (Illumina). Triplicates were sequenced for each condition in separate lines. Sequencing output was processed to generate FASTQ files for downstream analysis.

VAST-TOOLS splicing pipeline analysis

VAST-TOOLS[6] v.2.5.1 and the database vastdb.hs2.23.06.20 were used to identify alternative splicing events from RNA-seq data. For DU145, we generated single-end 50 bp reads (average of 46 million per sample) and paired-end 150 bp reads (average of 56 million per sample) datasets for 4 control (no DOX), and 4 samples after *AMD1* silencing for 2 days. Reads were mapped to the human genome (version GRCh38) using VAST-TOOLS align module (-IR_version 2 -stepSize 25 -mismatchNum 2). Aligned single and paired datasets were merged with the merge module. We combined the samples using 'combine' with parameters "-IR_version 2 -extra_eej 5". We identified differentially spliced events using Matt v.1.3.0 with minimum Abs(ΔPSI) > 10% and Wilcoxon *P* value < 0.1 after excluding events with PSIRANGE_ALL = NA and LENGTH = 0.

In the case of skeletal muscle RNA-seq analysis, reads were mapped to the mouse genome (version GRCm38) and vastdb.mm2.2306.20 database was used to identify alternative splicing events.

Neuroblastoma cell experiments

The neuroblastoma cell line SKNBE2 was cultured in RPMI (Gibco). To inhibit polyamine biosynthesis, cells were treated for 4 days with 250 µM of DFMO obtained from P. Woster. At sub-confluency cells were washed with ice-cold PBS and RNA was isolated from cell extracts by direct addition of 3-volumes of QIAzol (Qiagen, 79306). After thorough mixing, RNA was purified using the Direct-Zol RNA Mini Prep Plus kit. Stranded library preparation was performed at the Genomic Platform (UNIGE) following standard protocols. Libraries were sequenced on an Illumina NovaSeq 6000, SR 100 bp. In vivo experiments with Th-*Mycn* mice are described in ref. 12.

Analysis of functional relationships between AMD1 and splicing factors

To investigate functional relationships between AMD1 and splicing factors, we conducted a comparative analysis of splicing events affected by the knockdown of AMD1 and a comprehensive genome-wide screen of 304 splicing factors in HeLa cells, using a common threshold criteria. We considered splicing events that exhibited a change of at least 10% upon AMD1 knockdown, matching the threshold used in a transcription-wide screen of splicing factors.

To quantify the extent of shared splicing targets between AMD1 and the profiled splicing factors, we used the Jaccard index expressing the similarity between two sets calculated as the size of the intersection of the sets divided by the size of the union of the sets.

$$J(A, B) = |A \cup B||A \cap B|$$

We focused on matched splicing events, which were characterized by differences between control and experimental conditions not exceeding 15% for exonic events and 5% for other event types. Furthermore, we required that these splicing events exhibited a significant change of at least 5% and possessed a *P* value less than 0.05 in the knockdown of AMD1. To construct networks, we applied stringent similarity thresholds to ensure the biological relevance of identified associations. Specifically, we utilized a Jaccard score of 0.7 for exonic events and 0.67 for all other event types.

In vitro radiochemical CK1α assay

SF3A3 (Abnova, H00010946-P01), SF3A1 (Abnova, H00010291-P01) or SF3B2 (Abnova, H00010992-P01) recombinant proteins were pre-incubated 5 min with either vehicle (H_2O), Put (Sigma, P5780), Spd (Sigma, 85578), Spm (Sigma, S3256) or BENSpm (Tocris, 0468) when indicated, followed with incubation with 200 ng of active CKIα (Abcam, 102102) in kinase buffer (50 mM Tris/HCl pH 7.5, 0.1 mM EGTA, 0.1% (v/v) 2-mercaptoethanol). Reactions (total volume of 30 µl) were started by adding a mixture of 10 mM $MgCl_2$, 0.1 mM [γ-^{32}P]-ATP (500 cpm pmol^{-1}. Perkin-Elmer, BLU002A500UC). Assays were carried out for 30 min at 30 °C, and terminated by adding 5× Laemmli buffer and were heated at 95 °C for 5 min. Finally, proteins were resolved by SDS–PAGE gel electrophoresis, stained with Coomassie, and incorporation of ^{32}P into proteins was detected by autoradiography.

NMR

The SF3A3 fragment was produced in bacterial cells transformed with plasmid pET29a(+) containing a synthetic gene (Genscript) coding for residues 350–380 residues of the human protein (Uniprot 12874) fused at the N-terminal end to ubiquitin with a His_{10}-insertion for protein purification by immobilized metal affinity chromatography (IMAC) and followed by the TEV-protease cleavage sequence. Cultures were grown in auto-induction ZYP-5052 medium with kanamycin for protein production at 20 °C for 18 h. The fragment was purified by IMAC (5 ml His Trap column loaded with Co^{2+}, Cytiva), TEV cleavage, and reverse phase chromatography (C_{18} Jupiter 250 × 10 mm column, Phenomenex). The purity and the integrity of the fragment was evaluated by Coomassie-stained reducing SDS–PAGE, and by MALDI-TOF mass spectrometry. The purified fragment contains the non-native AGM sequence at the N-terminus. The SRRM1 synthetic lyophilized peptide with free termini was purchased from Apeptide. The sequence corresponds to residues 376–406 of the human protein (Uniprot Q8IYB3) with a non-native YG sequence at the N-terminus to measure its concentration by absorbance at 280 nm (as done with SF3A3).

All NMR experiments were performed using a Bruker 800 MHz spectrometer equipped with a cryoprobe. NMR data were processed with TopSpin (Bruker). ^{1}H NMR resonances of SF3A3 peptide were assigned through standard TOCSY and NOESY experiments of a sample containing SF3A3 peptide in 9:1 H_2O:D_2O at 630 µM concentration.

Reference spectra of the protein fragments without polyamines were recorded on 250 µM SF3A3 and 250 µM SRRM1 samples in 400 µl of 20 mM MES pH 7.0, H_2O:D_2O 9:1, inside a 5 mm Shigemi tube without plunger. Solutions of Put, Spd, Spm and N^1,N^{11}-bis(ethyl) norspermine at 360 mM and 1.75 M in 20 mM MES pH 7.0 were prepared by gravimetry. Volumes between 0.1 µl and 8.6 µl of one of the polyamine stocks were pipetted inside the NMR tube and mixed by capping and inverting the tube several times before recording the corresponding spectrum. Each titration was recorded in less than

two days. The chemical shift perturbations (CSPs) were quantified from NMR signals that were among the most perturbed, sufficiently intense, and not overlapping with other signals to measure their chemical shifts with high precision. They were computed at each point of the titration as $CSP = (((\Delta\delta H_N)^2 + (\Delta\delta H_\alpha)^2)/2)^{1/2}$), with an estimated error of ±0.005 ppm. The averaged values were fitted to a 1:1 binding model using GraphPad Prism to obtain the equilibrium dissociation constant.

Cell culture and photoaffinity labelling with Spd probe

The human cervical carcinoma cell line HeLa was maintained in Dulbecco's Modified Eagle Medium (DMEM, ATCC), supplemented with 10% fetal bovine serum (Thermo Fisher Scientific) and 1% penicillin/streptomycin (Thermo Fisher Scientific). Cells were grown at 37 °C with 5% CO_2 and routinely tested for mycoplasma infection (Universal Mycoplasma Detection Kit, ATCC). For photoaffinity labelling of proteins and protein pulldown, sub-confluent cells were washed with PBS and incubated with the Spd analogue[28] alkylated at the N8 position to attach the minimalist alkyl diazirine photo-crosslinker[29] in serum-free DMEM for 2 h or with serum-free DMEM without the addition of the analogue. The cells were washed with PBS and immediately irradiated (365 nm, 10+ mW cm^{-2}) for 10 min in PBS using an LED light reaction box (WaveyTech). Control cells were not UV irradiated, to exclude covalent probe-protein binding not related to the photoaffinity labelling. The cells were lysed with 2% SDS in PBS, probe-sonicated, and cysteine residues were reacted with 40 mM iodoacetamide for 40 min to prevent azide-alkyne-thiol reaction[37]. Proteins were precipitated by addition of methanol (1 volume) and chloroform (0.25 volumes), followed by a brief vortex-mixing. The pellets were washed with methanol twice, air-dried, and reconstituted in 2% SDS in PBS. The solutions were diluted with PBS to the final concentration of 0.5% SDS and the protein concentration was determined by DC Protein Assay (Bio-Rad) and normalized. Protein solutions were then subjected to the click reaction[38]. A click mixture was prepared by combining four reagents (volumes given per 100 µg of proteins) in the following order: 5-TAMRA-azide (Jena Bioscience) or azide-PEG3-biotin (Sigma-Aldrich) (1 µl, stock 10 mM in DMSO, final concentration 0.1 mM), $CuSO_4$ (2 µl, stock 50 mM in water, final concentration 1 mM), tris(2-carboxyethyl)phosphine (TCEP) (2 µl, stock 50 mM in water, final concentration 1 mM), tris((1-hydroxy-propyl-^{1}H-1,2,3-triazol-4-yl)methyl)amine (THPTA) (1 µl, stock 20 mM in water, final concentration 0.2 mM). The samples were incubated with the click mixture at room temperature for 1 h. EDTA (final concentration 5 mM), methanol (1 volume) and chloroform (0.25 volume) were added. The samples were quickly vortexed and centrifuged at 21,000*g* for 5 min to pellet precipitated proteins. The pellets were washed with methanol twice, and air-dried. TAMRA-labelled proteins were resolved by SDS–PAGE and visualized with Amersham Imager (Amersham). For the protein load determination, silver staining was performed with Pierce Silver Stain kit (Thermo Fisher Scientific). Biotin-labelled proteins were instead subjected to the pull-down with streptavidin beads (New England Biolabs) for 2 h at room temperature with 1,100 rpm shaking. After washing of non-specifically bound proteins, beads were boiled with Laemmli buffer for protein retrieval and samples were subjected to SDS–PAGE separation and western blot analysis with SF3A3 (Abcam, ab176581-100) and SF3B2 (Bethyl, A301-606A) specific antibodies.

Metabolomics

For tissue extraction, 500 µl of ice-cold extraction liquid was added with a tissue homogenizer (FastPrep) in one 40 s cycle at 6,000 rpm. The extraction liquid consisted of a mixture of ice-cold methanol/water (50/50% v/v) with 10 mM acetic acid. Subsequently, 400 µl of the homogenate plus 400 µl of chloroform was transferred to a new aliquot and shaken at 1,400 rpm for 30 min at 4 °C. Next the aliquots were centrifuged for 30 min at 13,000 rpm at 4 °C. The organic phase was separated from the aqueous phase. From the aqueous phase 300 µl was transferred to a fresh aliquot and placed at −80 °C for 20 min. The chilled supernatants were evaporated with a speedvac in approximately 2 h. The resulting pellets were resuspended in 250 µl water/acetonitrile (MeCN) (40%/60% v/v). Concentrations of metabolites were determined with a semi-quantitative method. Calibration curves for these compounds were obtained by measuring serial dilutions of a pooled standard mixture in resuspension solution. The concentrations for metabolites in the dilutions ranged from 100 µM to 0.025 µM, except for MTA which range was from 10 µM to 0.0025 µM. For the standard mixture, separate 10 mM stock of the standard was made. This was then diluted in resuspension solution to obtain the final concentrations as used for the calibration curve. Since the calibration solutions lacked any biological matrix, the method should be considered semi-quantitative.

Samples were measured with a UPLC system (Acquity, Waters) coupled to a Time-of-Flight mass spectrometer (ToF MS, SYNAPT G2S, Waters). A 2.1 × 100 mm, 1.7 µm BEH amide column (Waters), thermostated at 40 °C, was used to separate the analytes before entering the MS. Mobile phase solvent A (aqueous phase) consisted of 99.5% water, 0.5% formic acid and 20 mM ammonium formate while solvent B (organic phase) consisted of 29.5% water, 70% MeCN, 0.5% formic acid and 1 mM ammonium formate.

In order to obtain a good separation of the analytes the following gradient was used: from 5% A to 50% A in 2.4 min in curved gradient (no. 8, as defined by Waters), from 50% A to 99.9% A in 0.2 min constant at 99.9% A for 1.2 min, back to 5% A in 0.2 min. The flow rate was 0.250 ml min^{-1}, and the injection volume was 4 µl for the cell samples and 2 µl for media samples. After every 10 injections a quality control sample was injected.

The MS was operated in positive electrospray ionization mode in full scan (50 Da to 1,200 Da). The cone voltage was 25 V and capillary voltage was 1 kV. Source temperature was set to 120 °C and capillary temperature to 450 °C. The flow of the cone and desolvation gas (both nitrogen) were set to 5 l h^{-1} and 1,000 l h^{-1}, respectively. A 2 ng ml^{-1} leucine-enkephalin solution in water/acetonitrile/formic acid (49.9/50/0.1% v/v/v) was infused at 10 µl min^{-1} and used for a lock mass which was measured each 36 s for 0.5 s. Spectral peaks were automatically corrected for deviations in the lock mass.

Extracted ion traces for relevant analytes were obtained in a 20 mDa window in their expected *m/z* channels. These traces were subsequently smoothed and peak areas integrated with TargetLynx software (Waters).

These calculated raw signals for cells were adjusted by median fold-change (MFC) adjustment. This is a robust adjustment factor for global variations in signal due to, for example, difference in tissue amounts, signal drift or evaporation. MFC values are based on the total amount of detected mass spectrometric features (unique retention time/mass pairs) over all samples. The calculations and performance of the MFC adjustment factors are described elsewhere[39,40]. The polyamine cell extraction and quantification methodology using LC–MS measurements is detailed in[41].

Proteomics and phosphoproteomics

DU145 sh*AMD1* cells were grown in 150 mm plates and treated for 1 day or 2 days with doxycycline (100 ng ml^{-1}) to genetically silence *AMD1* (final density no higher than 60–70%).

Samples were lysed in 5% SDS, digested with trypsin using the standard S-TrapTM protocol and labelled using TMT reagent 11-plex. For phosphoproteome analysis, phosphopeptides were first purified using TiO_2 and then fractionated into six fractions using high pH reverse-phase home-made micro-column. For whole proteome analysis, the flow-through was fractionated using high pH reverse-phase HPLC system and then, concatenated into 15 fractions. Samples were analysed by LC–MS/MS analysis using a Q-exactive HF-X mass spectrometer (Thermo Scientific). Raw files were analysed with MaxQuant

v.1.6.1.0 against a human protein database (UniProtKB/Swiss-Prot, 20,187 sequences downloaded on August 2016). Statistical analysis was done using Prostar v.1.12.14 and Perseus v.1.6.7. GO analysis: Functional enrichment analysis was done with G: profiler (https://biit.cs.ut.ee/gprofiler/gost) using the GO database. Multiple testing correction (SCS threshold) was applied and only terms with an adjusted *P* value below 0.05 were considered as significant. GO terms containing less than 100 genes or more than 500 genes were discarded. Motifs: Enrichment of specific amino acids surrounding the identified phosphorylation sites was done with IceLogo using a *P* value threshold of 0.001 (https://iomics.ugent.be/icelogoserver). Aa conservation: Protein sequences were retrieved from Uniprot and aligned using the clustalo algorithm (v.1.2.4). Residues are shown using the Clustal2 colour scheme. The surface accessibility, secondary structure, disorder, and phi/psi dihedral angles of amino acids in protein sequences were predicted with NetSurfP server (https://services.healthtech.dtu.dk/services/NetSurfP-2.0/). Kinase prediction was done with the GPS 6.0 tool (available at http://gps.biocuckoo.cn/), Networkin 3.0 and Phosphositeplus[42,43].

For pharmacological inhibition and polyamine rescue in DU145 and HeLa experiments cells were grown in 100 mm plates and treated for 2 days with SAM486A (1 μM) + DFMO (50 μM) or SAM486A + DFMO+ polyamines (10 μM). Samples were lysed in 2% SDS, digested with trypsin/Lys-C mix (Promega) using the standard SP3 protocol[44,45] and labelled using TMT reagent 18-plex (ThermoFisher). For whole proteome analysis, a small aliquot was fractionated into eight fractions using Pierce high pH reverse-phase peptide fractionation kit (ThermoFisher). For phosphoproteome analysis, phosphopeptides were first purified using MagReSyn Zr-IMAC HP beads and then fractionated using the same procedure as for the whole proteome. Samples were then analysed by LC–MS/MS analysis using a Vanquish Neo LC system coupled to an Exploris 480 mass spectrometer (Thermo Scientific). Raw files were analysed with MSFragger v.22.0 against a human protein database (UniProtKB/Swiss-Prot, 20,836 sequences downloaded in May 2024). Statistical analysis was done using Prostar v.1.34.6 and Perseus v.2.0.10.0. GO analysis: Functional enrichment analysis was done with G: profiler (https://biit.cs.ut.ee/gprofiler/gost) using the GO database. Multiple testing correction (SCS threshold) was applied and only terms with an adjusted *P* value below 0.05 were considered as significant. GO terms containing less than 100 genes or more than 500 genes were discarded. The isoelectric point of each phosphopeptide was calculated using the Expasy Compute pI/Mw tool (https://web.expasy.org/compute_pi/).

Mouse ES cell culture

Mouse ES cells were generated previously from C57BL/6 × 129S4/SvJae F_1 male mouse embryos[46]. Nanog–GFP ES cells were a gift from R. Jaenisch[47]. For all experiments, ES cells were maintained on gelatin-coated plates in serum medium containing leukaemia inhibitory factor (LIF) (S/L medium). S/L medium was composed of knockout DMEM (10829018, Thermo Fisher Scientific) supplemented with 10% FBS (Gemini), 0.1 mM 2-mercaptoethanol, 2 mM L-glutamine, and 1,000 U ml^{-1} LIF (Gemini). For −LIF conditions, LIF or pharmacological manipulation of polyamine metabolism, ES cells were treated with the following drugs for 48 h: DFMO (50 μM in methanol), *S*-adenosylmethionine (0.5 μM in ethanol) and BENSpm (10 μM in water). Methanol or ethanol were used as vehicle controls.

Nanog–GFP analysis

To assess the effect of polyamine synthesis inhibition on Nanog–GFP distribution, Nanog–GFP ES cells, a gift from R. Jaenisch (Whitehead Institute for Biomedical Research)[47], were seeded at a density of 55,000 cells per well of a 12-well plate in culture medium with or without LIF supplementation. After 48 h, the cells were detached with 0.5 g l^{-1} trypsin-EDTA and resuspended in flow cytometry buffer (PBS with 2% FBS, 0.5 mM EDTA and 0.05% sodium azide) with DAPI. GFP signal was measured on an LSRFortessa flow cytometer using FACSDiva software (v.8.0) (BD Biosciences) and analysed using FlowJo (v.10.9.0).

Collection of mouse ES cells for RNA-seq

ES cells were seeded at a density of 150,000 cells in 6-well plates. Cells were cultured in S/L medium or in LIF withdrawn medium for 48 h prior to collection. After 48 h, cells were washed in PBS and collected in 1 ml TRIzol (Invitrogen).

Collection of mouse ES cells for metabolomics

ES cells were seeded at a density of 150,000 cells in 6-well plates. Cells were cultured in S/L medium or in LIF withdrawn medium for 48 h prior to collection. After 48 h, cells were scraped in PBS, pelleted, and snap froze until further processing. In parallel, cells were collected in 1 ml NP-40 for protein normalization.

Statistical analysis and reproducibility

The sample size was determined without using statistical methods. The experiments were not randomized, and investigators were aware of the allocation during both the experiments and outcome assessment. When analysing data using parametric tests, results are presented as mean ± s.e.m. from pooled experiments, unless otherwise specified. For non-parametric datasets, values are represented as median with interquartile range. The *n* values indicate the number of independent biological experiments performed or the number of individual mice analysed, as specified in each figure legend.

For in vitro experiments, a minimum of two technical replicates were included, and at least three independent biological experiments were performed to ensure robust statistical power. This applies to semi-quantitative PCR analyses (gel densitometry), RT–qPCR, western blot experiments and photoaffinity labelling with the Spd probe, all of which were replicated at least three independent times, with statistics derived from biological replicates. Representative blots are shown. In vitro radiochemical CK1α kinase assays were performed independently at least twice.

Flow cytometry analyses in ES cells were performed in two independent biological experiments, and the statistics presented in bar plots were obtained from technical replicates of a representative experiment.

For in vitro analyses, normal distribution was assumed. One-sample *t*-tests with the corresponding hypothetical value (1 or 100) were routinely used for normalized datasets. For two-group comparisons of relative values, paired Student's *t*-tests were applied. For experiments without a predicted outcome, two-tailed analyses were used, while one-tailed tests were used for validation or hypothesis-driven experiments. The confidence level for all statistical analyses was set at 95% ($\alpha = 0.05$). Statistical analyses were performed using GraphPad Prism software.

NMR experiments were acquired once per condition due to the inherently high reproducibility of NMR spectroscopy. Sample stability throughout titration series was confirmed by ^{1}H-NMR. All measurements were performed under controlled pH, temperature and concentration conditions, with constant acquisition and processing parameters to ensure chemical-shift consistency and comparability.

Metabolomic, phosphoproteomic and RNA-seq datasets were generated from at least three independent biological replicates or samples.

For all in vivo experiments, the minimum number of mice analysed per group was four, as reported in the corresponding figure legends.

All uncropped and unprocessed scans of blots have been provided in the Supplementary Information.

Reporting summary

Further information on research design is available in the Nature Portfolio Reporting Summary linked to this article.

Data availability

The mass spectrometry proteomics data have been deposited to the ProteomeXchange Consortium via the PRIDE partner repository with the dataset identifiers PXD046107 for DU145 sh*AMD1* data and PXD065659 for DU145 and HeLa cells treated with SAM486A and DFMO with and without polyamine. For in vitro data in SKNBE2 cells treated with DFMO, sequence data have been deposited at the Gene Expression Omnibus (GEO) under accession GSE301290, and in vivo sequence data for Th-*Mycn* cells injected in mice and treated with DFMO the GEO accession is GSE244378 (originally reported in ref. 12). The remaining RNA-seq data are available from GEO accession GSE255769. Source data are provided with this paper.

Code availability

Codes for molecular modelling data analysis can be accessed through Zenodo at https://zenodo.org/records/17008960 (ref. 48). Codes for the alternative splicing analysis based on RNA-seq data can be accessed through Zenodo at https://doi.org/10.5281/zenodo.17020551 (ref. 49). Code for the networks is available from ref. 50 (https://github.com/estepi/SpliceNet).

34. Pease, S. & Saunders, T. L. (eds). *Advanced Protocols for Animal Transgenesis* (Springer, 2011).
35. Torrano, V. et al. The metabolic co-regulator PGC1α suppresses prostate cancer metastasis. *Nat. Cell Biol.* **18**, 645–656 (2016).
36. Wiederschain, D. et al. Single-vector inducible lentiviral RNAi system for oncology target validation. *Cell Cycle* **8**, 498–504 (2009).
37. Wiest, A. & Kielkowski, P. Cu-catalyzed azide–alkyne–thiol reaction forms ubiquitous background in chemical proteomic studies. *J. Am. Chem. Soc.* **146**, 2151–2159 (2024).
38. Rostovtsev, V. V., Green, L. G., Fokin, V. V. & Sharpless, K. B. A stepwise huisgen cycloaddition process: copper(I)-catalyzed regioselective "ligation" of azides and terminal alkynes. *Angew. Chem. Int. Ed.* **41**, 2596–2599 (2002).
39. Dieterle, F., Ross, A., Schlotterbeck, G. & Senn, H. Probabilistic quotient normalization as robust method to account for dilution of complex biological mixtures. Application in ^{1}H NMR metabonomics. *Anal. Chem.* **78**, 4281–4290 (2006).
40. Veselkov, K. A. et al. Optimized preprocessing of ultra-performance liquid chromatography/mass spectrometry urinary metabolic profiles for improved information recovery. *Anal. Chem.* **83**, 5864–5872 (2011).
41. Cabrera, D. et al. Development and validation of a precise and accurate method to determine polyamine levels in cultured cells. Preprint at *bioRxiv* https://doi.org/10.1101/2025.05.29.654479 (2025).
42. Johnson, J. L. et al. An atlas of substrate specificities for the human serine/threonine kinome. *Nature* **613**, 759–766 (2023).
43. Linding, R. et al. Systematic discovery of in vivo phosphorylation networks. *Cell* **129**, 1415–1426 (2007).
44. Hughes, C. S. et al. Ultrasensitive proteome analysis using paramagnetic bead technology. *Mol. Syst. Biol.* **10**, MSB145625 (2014).
45. Hughes, C. S. et al. Single-pot, solid-phase-enhanced sample preparation for proteomics experiments. *Nat. Protoc.* **14**, 68–85 (2019).
46. Carey, B. W., Finley, L. W., Cross, J. R., Allis, C. D. & Thompson, C. B. Intracellular α-ketoglutarate maintains the pluripotency of embryonic stem cells. *Nature* **518**, 413–416 (2015).
47. Faddah, D. A. et al. Single-cell analysis reveals that expression of Nanog is biallelic and equally variable as that of other pluripotency factors in mouse ESCs. *Cell Stem Cell* **13**, 23–29 (2013).
48. Zabala-Letona, A. et al. Polyamine-dependent metabolic shielding regulates alternative splicing [Data set]. *Zenodo*. https://doi.org/10.5281/zenodo.17008960 (2025).
49. Mendizabal, I. & Ponce Rodríguez, M. Script repository: polyamine-dependent metabolic shielding regulates alternative splicing (https://github.com/imendizabalCIC/Polyamine_AlternativeSplicing). *Zenodo* https://doi.org/10.5281/zenodo.17020551 (2025).
50. Rogalska, M. E. et al. Transcriptome-wide splicing network reveals specialized regulatory functions of the core spliceosome. *Science* **386**, 551–560 (2024).

Acknowledgements We thank the Carracedo laboratory for valuable input; M. González, L. Barcena and N. Macias for technical support. The work of A.C. is supported by the MICIU (PID2022-141553OB-I0 (FEDER/EU), BBVA foundation Leonardo Grant for Scientific Research and Cultural Creation (Beca Leonardo LEO23-2-10984-BBM-TRA-261), Fundación Cris Contra el Cáncer (PR_EX_2021-22), Severo Ochoa Excellence Accreditation (CEX2021-001136-S), Fundación AECC (Excelencia 2024 call, Premetacan—EPAEC246710BIO), Fundación Occident, Astrazeneca Foundation (Young Oncologist award), Vencer el Cáncer Foundation, Mondravember, iDIFFER Network of Excellence (RED2022-134792-T; RED2024-153635-T), and the European Research Council (Consolidator Grant 819242). CIBERONC was co-funded with FEDER funds and ISCIII. A.Z.-L. is supported by AECC (INVES223210ZABA). M.P.-V. was supported by a Basque Government PhD training fellowship and CIBER. B.M.-L. and M.A.-C. were supported by FPI fellowships (MCIU). M.F.-E. was supported by Basque Government PhD training fellowship. A. Ercilla is supported by a Juan de la Cierva Incorporación fellowship from the MCIN/AEI /10.13039/501100011033. L.B.-B. was supported by the AECC Foundation (POSTD19048BOZA). M.Z. and R.A.S. are supported by the National Science Centre, Poland (grant no. 2020/38/E/ST4/00250). I.M. is supported by Fundación Cris Contra el Cáncer (PR_TPD_2020-19) and a Ramón y Cajal contract (RYC2023-044682-I) funded by the MCIU. G.J.-O. was funded by the MICIU (PID2021-125946OB-I00 and PDC2022-133725-C22). F.P. was funded by the MICIU (IJC2020-045506-I) and RYC (RYC2022-036457-I). F.J.B. was funded by PID2023-147699OB-I00 grant from AEI- /10.13039/501100011033. The work of A.R. is partially supported by the Basque Department of Industry, Tourism and Trade (Elkartek). The laboratory of J.M. is supported by the European Union Horizon 2020 programme INFRAIA project EPIC-XS (project 823839). S.C. and R.J.M. were supported by grants from the NOMIS Foundation and Geistlich-Stucki Stiftung. R.B. and J.D.S. were funded by PID2020-114178GB-I00 and PID2023-147399NB-I00 (MINECO /MICINN/FEDER, EU). E.B. is supported by the PID2022-141556OB-I00 (FEDER/EU) and RED2022-134407-T). A. Efeyan is funded by grant PID2022-136413OB-I00. The laboratory of J.M.L. is funded by the MICIU (PID2022-136391OB-I00). The work of L.F. was supported by Memorial Sloan Cancer Center Support Grant P30CA008748. The work from R.J.M. in this publication is based on work from COST Action Translational control in Cancer European Network (TRANSLACORE) CA21154 supported by COST (European Cooperation in Science and Technology). M.D.H. was supported by a US Department of Defense Team Translational Science Award (CA170257).

Author contributions A.Z.-L. and M.P.-V. performed and coordinated the majority of in vitro and in vivo experiments, unless specified otherwise. B.M.-L. performed in vitro experiments of pharmacological inhibitors and BENSpm. I.M., M.P.-R. and M.R. performed and coordinated all the splicing analysis. P.X.-E., M.S. and J.M. contributed to the design and/or executed the phosphoproteomic analysis. S.E. and J.M.L. executed and designed the kinase assays. F.P. and G.J.-O. performed molecular docking and molecular dynamics simulations. J.A.F.-B., F.C., C.L. and A.R. performed in silico RNA-binding protein enrichment analysis. N.M.-M. contributed to the cell culture of different cell lines in vitro experiments. M.F.-E. provided support in the execution of semiquantitative PCR for splicing events validation in cell lines treated with SAM486A and executed experiments of cells in hypoxia designed by E.B. I.M.-B., F.J.B., A.G. and J.J.-B. designed and performed NMR assays. I.A., M.A.-C., A. Ercilla, L.B.-B., O.C., T.S.-Z., A.A.-A., E.P.-A., S.G.-L., A.M.A., R.B., J.D.S. and J.S. provided technical support and critical discussions. B.M.-P. and A. Efeyan designed and executed *Sf3a3*$^{KI/KI}$ mouse generation, and experiments related to mouse embryonic fibroblasts. S.C., M.D.H. and R.J.M. designed and performed in vitro experiments in neuroblastoma cells and provided transcriptomics data from neuroblastoma in vivo experiment. M.Z., M.C. and R.A.S. synthesized the Spd probe and performed photoaffinity labelling experiments. D.C., S.v.L. and J.M.F.-P. designed and performed polyamine metabolomics quantification assays. J.T. and L.F. designed and performed experiments with ES cells. J.V. supported the splicing analysis strategy, analysed the results, and contributed to critical discussions and manuscript preparation. A.C. conceived and directed the project, supervised data analysis and wrote the manuscript.

Competing interests The authors declare no competing interests.

Additional information

Supplementary information The online version contains supplementary material available at https://doi.org/10.1038/s41586-025-09965-1.

Correspondence and requests for materials should be addressed to Arkaitz Carracedo.

Peer review information *Nature* thanks the anonymous reviewer(s) for their contribution to the peer review of this work. Peer review reports are available.

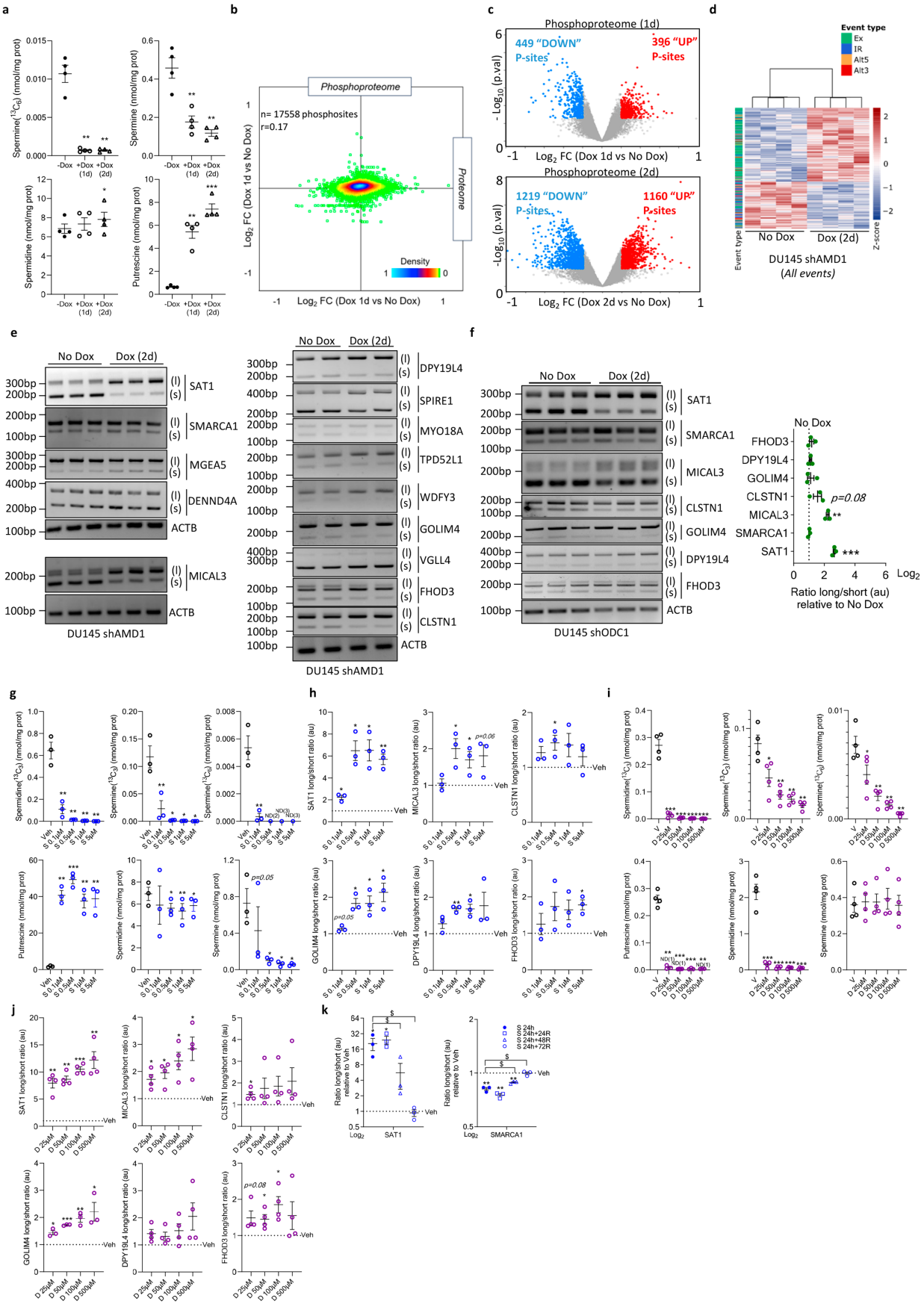

Extended Data Fig. 1 | See next page for caption.

Extended Data Fig. 1 | Phosphoproteomic and transcriptomic analysis reveal alternative splicing as a molecular process modulated upon PA deprivation in DU145 cells. a, LC-MS analysis showing spermine levels assessed via incorporation of [^{13}C]-methionine and total polyamine levels (putrescine, spermidine, and spermine) in DU145 cells after 1 and 2 days of doxycycline-inducible *AMD1* silencing (100 ng/mL). **b**, Two-dimensional density plot showing the effect of *AMD1* inducible silencing (1 day) in the phosphoproteome (X axis) vs proteome (Y axis). **c**, Volcano plot representation of the number of phosphosites changing upon *AMD1* inducible silencing for 1 day (above) or 2 days (below). Statistical analysis was done using Prostar v1.12.14 and Perseus v1.6.7. **d**, z-scored PSI heat map depicting alternative splicing events (all events) altered upon *AMD1* inducible silencing for 2 days in DU145 cells (Abs(ΔPSI) > 10 %, p < 0.1). **e**, Experimental validation by semi-quantitative PCR of top alternative splicing exonic events altered upon *AMD1* silencing at 2 days in DU145 cells. **f**, Semi-quantitative PCR (left) and densitometry quantification as long/short transcript ratios (right) validating top AS events altered following *ODC1* inducible silencing with doxycycline (150 ng/mL) for 2 days in DU145 cells. **g**, **h**, Dose-dependent effects of AMD1 pharmacological inhibition (SAM486A, 48 h) on polyamine metabolism and splicing: (**g**) LC-MS analysis of methionine-derived [^{13}C] incorporation (top) and total polyamines (bottom), (**h**) densitometry quantification of long/short transcript ratios of AS events. **i**, **j**, Dose-dependent effects of ODC1 pharmacological inhibition (DFMO, 48 h) on polyamine metabolism and splicing: (**i**) LC-MS analysis of methionine-derived [^{13}C] incorporation (top) and total polyamines (bottom), (**j**) densitometry quantification of long/short transcript ratios of AS events. **k**, Densitometry quantification of long/short transcript ratios of AS events in DU145 cells treated with SAM486A (0.5 μM, 24 h) and recovered after drug washout (24–72 h). Abbreviations: Dox: doxycycline, S: SAM486A, D: DFMO, R: release, Veh: vehicle. Statistics: One-tailed paired student's t-test is used for analysis of metabolomics data in (**a**, **g**, **i**). One-tailed one sample t-test is applied in panels (**f**, **h**, **j**, **k**) p: p-value. One-tailed one sample t-test is applied in panels (**f**, **h**, **j**, **k**). p: p-value. *p < 0.05, **p < 0.01, ***p < 0.001. Dollars: represent a one-tailed paired t-test of the effect of SAM486A vs SAM486A + different time points of drug washout. $ p < 0.05. Error bars: Mean ± S.E.M. n= independent biological replicates (**a**, **i**, **j**: 4; **e**: 3-4; **f**, **g**, **h**, **k**: 3).

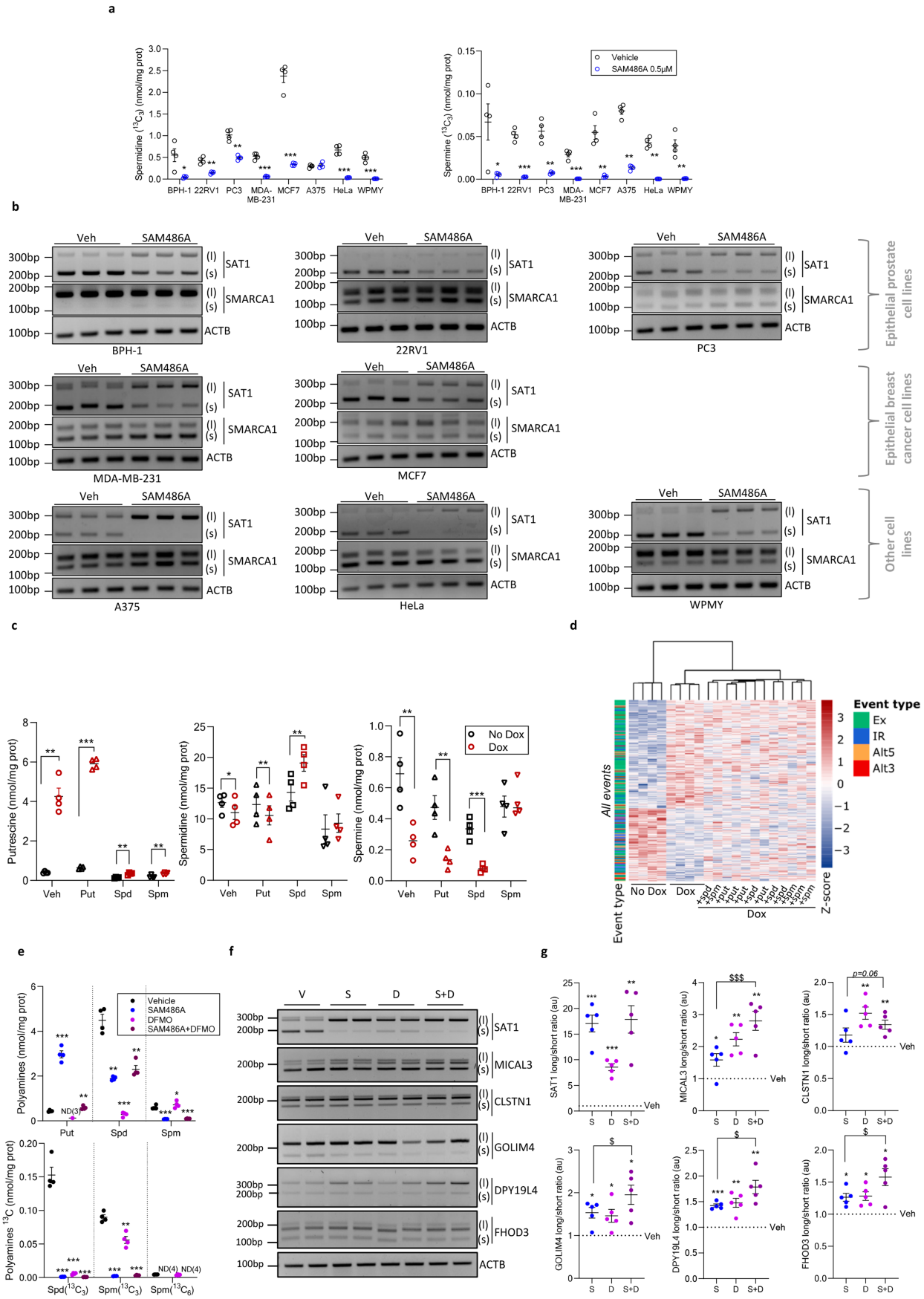

Extended Data Fig. 2 | See next page for caption.

Extended Data Fig. 2 | Alteration of alternative splicing upon inhibition of polyamine synthesis is consistent across cell lines and rescued by polyamine supplementation. a, **b**, LC-MS analysis of [^{13}C]-methionine incorporation in spermidine and spermine (**a**), and semi-quantitative PCR analysis of alternative splicing events (**b**) in various cell lines treated with SAM486A (0.5 μM) for 48 h. **c**, **d**, Quantitative LC-MS analysis of polyamines (**c**), and z-scored (Abs(ΔPSI) > 10%, adj-p < 0.1) heat map of AS events (all events) (**d**) in DU145 sh*AMD1* cells treated with doxycycline (100 ng/mL, 2 days) and individually supplemented with putrescine, spermidine, or spermine (10 μM each) (Abs(ΔPSI) > 10 %, p < 0.1). **e**-**g** LC-MS metabolomics of total polyamines (putrescine, spermidine, spermine) (top) and methionine-derived [^{13}C] incorporation (bottom) (**e**), semi-quantitative PCR gel of alternative splicing events (**f**), and densitometric quantification of long/short transcript ratios (**g**) showing the effects of SAM486A (1 μM, 48 h), DFMO (50 μM, 48 h), or their combination in DU145 cells. Abbreviations: Dox: doxycycline, ND: non-detectable, S: SAM486A; D: DFMO. Statistics: One-tailed student's paired t-test was used for panel (**a**, **c**, **e**). One-tailed one-sample t-test was applied in panel (**g**). p: p-value. *p < 0.05, **p < 0.01, ***p < 0.001. Dollars represent a two-tailed paired t-test of the effect of SAM486A *vs* SAM486A + DFMO (**g**). $ p < 0.05, $$$ p < 0.01. Error bars: Mean ± S.E.M. n= independent biological replicates (**a, c, e**: 4; **b**: 3; **f**, **g**: 5).

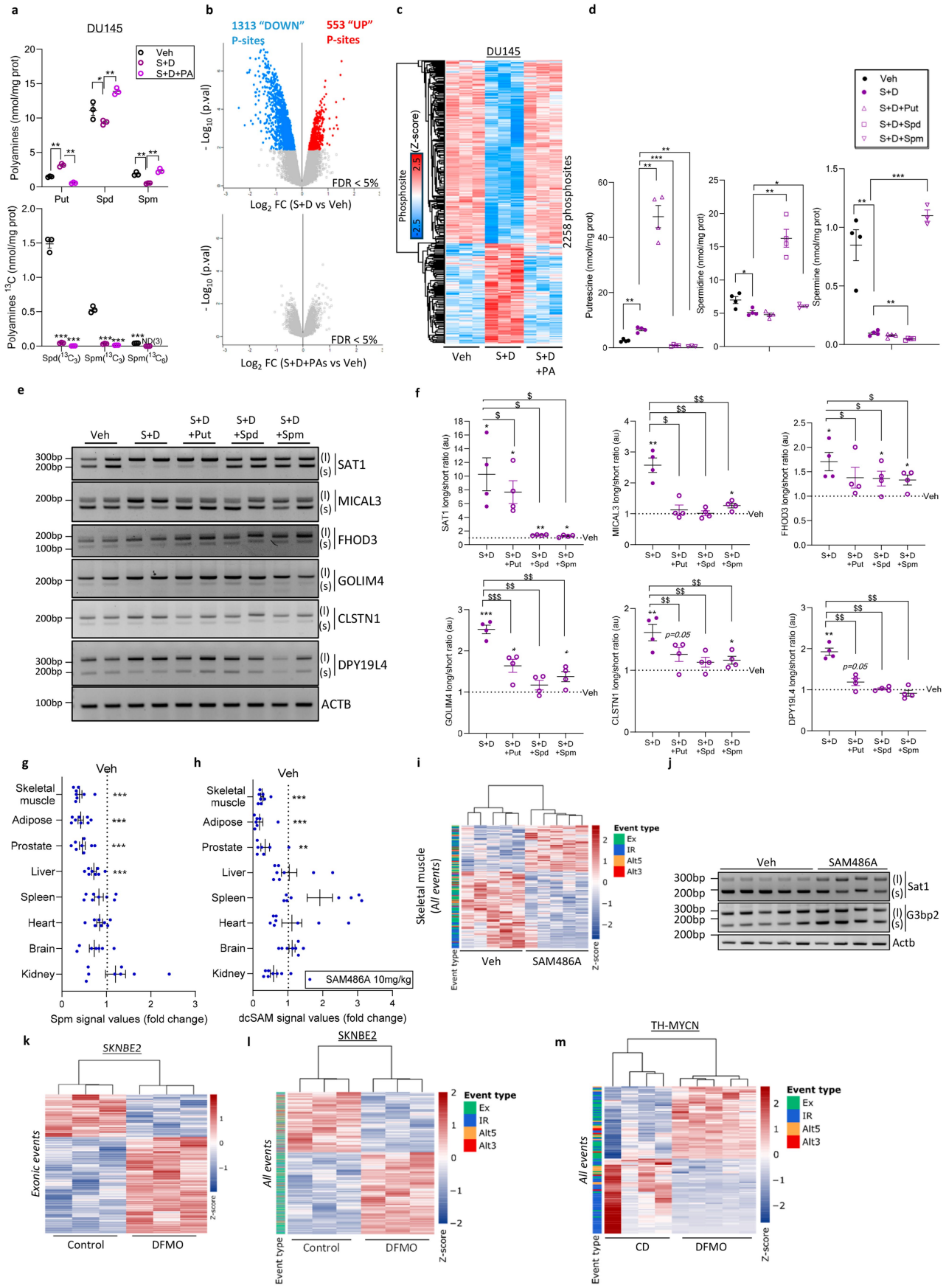

Extended Data Fig. 3 | See next page for caption.

Extended Data Fig. 3 | Consequences of pharmacological perturbation of polyamine biosynthesis on the phosphoproteome and alternative splicing in vitro and in vivo. a, LC-MS of polyamine levels in DU145 cells treated with SAM486A + DFMO (1 μM, 50 μM) or SAM486A + DFMO plus exogenous polyamines (10 μM each, 48 h). Total polyamines (top) and [^{13}C]-methionine incorporation into spermidine/spermine (bottom). **b**, Volcano plots of phosphoproteomic changes in DU145 cells after SAM486A + DFMO vs vehicle (top), and SAM486A + DFMO + exogenous polyamines vs vehicle (bottom). Statistical analysis was done using Prostar v1.12.14 and Perseus v1.6.7. **c**, Heatmap of Z-scored phosphosite abundance (Abs(ΔPSI) > 10 %, adj-p < 0.1) in DU145 cells treated with SAM486A + DFMO ± exogenous polyamines (48 h). **d-f**, LC-MS metabolomics of polyamines (**d**), semi-quantitative PCR of AS events (**e**), and densitometry of long/short transcript ratios (**f**) in DU145 cells treated with the combination of SAM486A (1 μM, 48 h) + DFMO (50 μM, 48 h), or S + D with rescue by individual polyamines (10 μM, 48 h). **g**, **h**, LC-MS metabolomics analysis of spermine (**g**) and decarboxylated S-adenosylmethionine (dcSAM) (**h**) levels in various tissues of male mice (mix background) treated with SAM486A (10 mg/kg) for 8 days. **i**, **j**, z-scored (Abs(ΔPSI) > 10%, adj-p < 0.1) heat map representation of alternative splicing events (**i**) and semi-quantitative PCR for selected splicing events (*Sat1, G3bp2*) (**j**) in skeletal muscle from mice treated as in (**g**, **h**). **k**, **l**, z-scored (Abs(ΔPSI) > 10%, adj-p < 0.1) heat map representation of RNA-seq based on exonic splicing events (**k**) and all events (**l**) in SKNBE2 neuroblastoma cells treated with 250 μM DFMO for 4 days. **m**, z-scored PSI heat map representation of alternative splicing events in TH-MYCN mice treated with DFMO. Abbreviations: FDR: false discovery rate, S: SAM486A, D: DFMO. CD: Control Diet. ND: non-detectable. Statistics: One-tailed paired student's t-test for metabolomics (**a**, **d**); one-tailed one-sample t-test in (**f**, **g**, **h**). *p < 0.05, **p < 0.01, ***p < 0.001. Dollars: two-tailed paired t-test comparing S + D vs S + D+putrescine/spermidine/spermine (**f**). $ p < 0.05, $$ p < 0.01, $$$ p < 0.001. Error bars: Mean ± S.E.M. n= independent biological replicates (**a**: 3; **d**, **e**, **f**: 4). n= independent mice (9 Veh and 8 SAM486A in **g**, **h**; 5 Veh and 5 SAM486A in **i**; 5 Veh and 4 SAM486A in **j**; 4 Control and 5 DFMO in **m**).

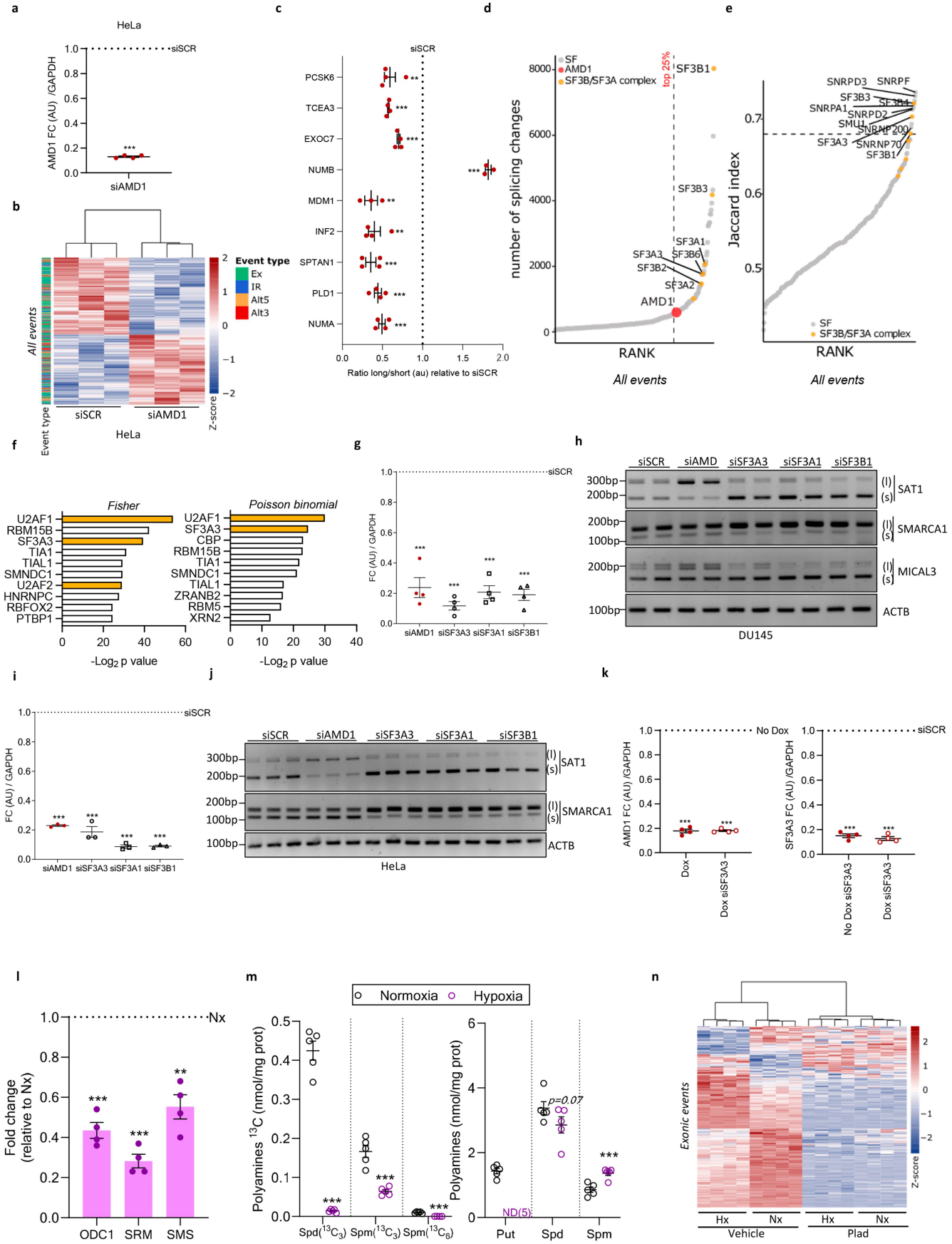

Extended Data Fig. 4 | See next page for caption.

Extended Data Fig. 4 | The SF3 subcomplex is relevant for polyamine-deprivation-induced alterations in alternative splicing. a, RT-qPCR analysis of the silencing efficiency of siRNA targeting *AMD1* (2 days) in HeLa cells. **b**, z-scored PSI heat map representation of *AMD1* siRNA silencing effect in AS of all events in HeLa cells (Abs(ΔPSI) > 10 %, adj-p < 0.1). **c**, Quantification by densitometry and representation of the relative long/short transcripts ratio of the top AS exonic events arising from the analysis of the RNA sequencing in HeLa cells (si*AMD1* vs si*SCR*). **d**, Scatter plot showing the number of all splicing changes induced with the silencing of *AMD1* or the different *SFs* on HeLa cells. **e**, Jaccard index rank plot of all the AS events shared between AMD1 silencing (si*AMD1* vs si*SCR*) and each of the individual splicing factors silencing compared to their si*SCR*. **f**, CLIP-based bar plots of splicing factors (SFs) with mRNA binding sites and splicing perturbations compatible with AMD1 silencing in DU145 cells. VAST-TOOLS pipeline applied with Fisher and Poisson Binomial tests. In yellow highlighted U2 snRNP associated members. **g**, **h**, Silencing efficiency of siRNAs targeting *AMD1, SF3A3, SF3A1* and *SF3B1* (**g**) and semi-quantitative PCR gels upon *AMD1* and *SF3* component siRNA silencing (2 days) vs siSCR in DU145 cells (**h**). **i**, **j**, Silencing efficiency of siRNAs targeting *AMD1, SF3A3, SF3A1* and *SF3B1* (**g**) and semi-quantitative PCR gels upon *AMD1* and *SF3* component siRNA silencing (2 days) vs siSCR in HeLa cells. **k**, RT-qPCR analysis of the silencing efficiency of sh*AMD1* and si*SF3A3* at transcriptional level. **l**, **m**, qPCR analysis of polyamine synthesis related genes (**l**) and LC-MS quantification of PAs by means of methionine-derived [^{13}C] incorporation (left) and total polyamine levels (right) (**m**) in DU145 cells exposed to hypoxia (1% O_2) for 24 h compared to normoxia (21% O_2). **n**, z-scored (Abs(ΔPSI) > 10 %, adj-p < 0.1) heat map representation of alternative splicing exonic events in DU145 cells submitted to hypoxia (1% O_2) or normoxia (21% O_2) for 24 h with or without Pladienolide B (10 nM, 24 h). Abbreviations: SCR: Scramble, SF: Splicing factor, Nx: normoxia, Hx: hypoxia, Plad: pladienolide. ND: non-detectable. Statistics: One-tailed one sample t-test with 1 as hypothetical value is applied in (**a**, **c**, **g**, **i**, **k**, **l**), one-tailed paired student's t-test is used for analysis of metabolomics data in (**l**). p: p-value. *p < 0.05, **p < 0.01, ***p < 0.001. Error bars: Mean ± S.E.M. n= independent biological replicates (**a**, **g**, **h**, **k**, **l**: 4; **c**: 3-4; **i**, **j**:3; **m**:5).

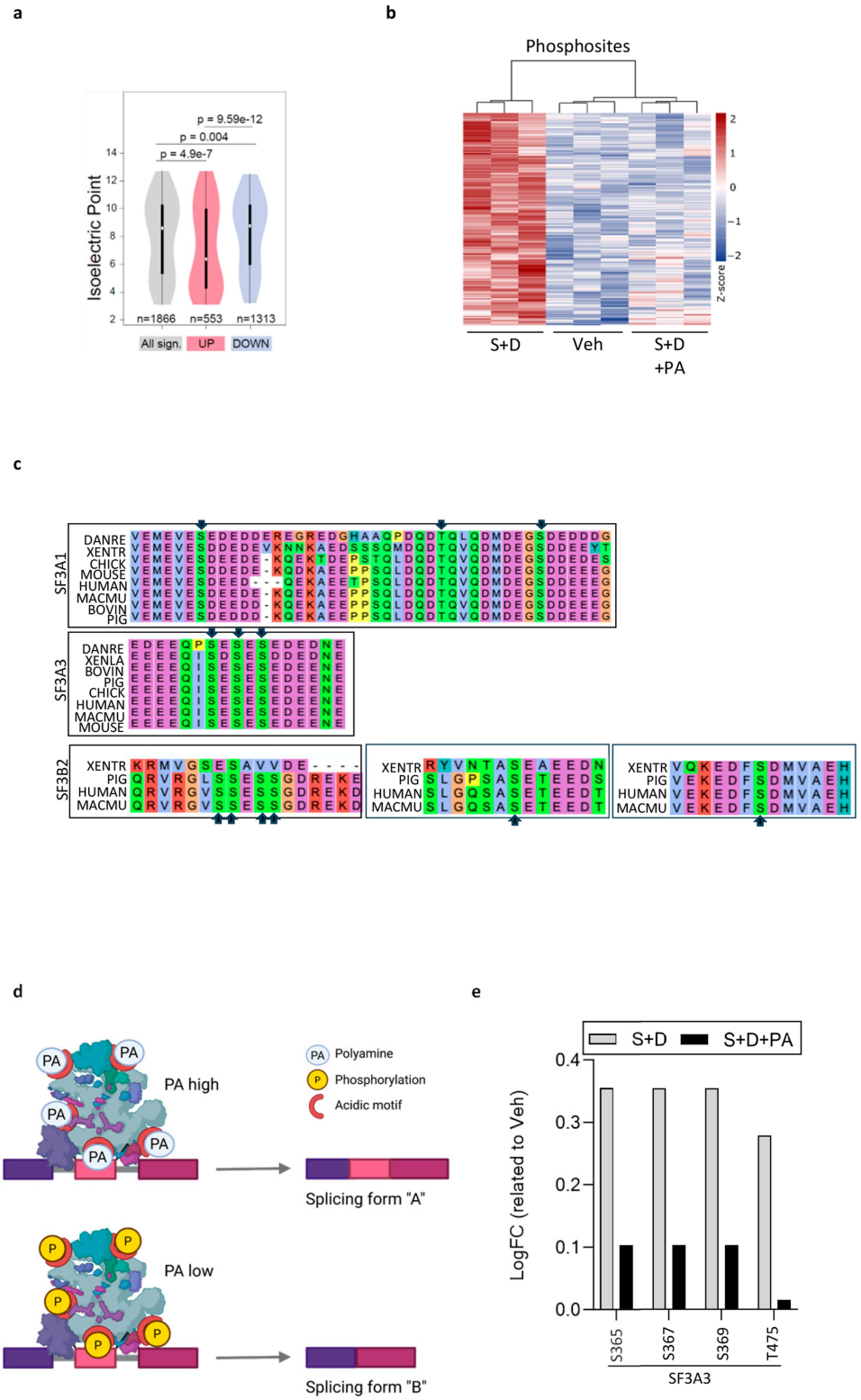

Extended Data Fig. 5 | See next page for caption.

Extended Data Fig. 5 | U2 snRNP SF3 phosphorylatable motifs are conserved and surface-accessible. a, Violin plot representation of the isoelectric points of significantly altered phosphopeptides in DU145 cells upon polyamine deprivation (SAM486A 1 µM + DFMO 50 µM, 48 h). White circles show the medians; box limits indicate the 25th and 75th percentiles; whiskers extend 1.5 times the interquartile range from the 25th and 75th percentiles and polygons represent density estimates of data and extend to extreme values. **b**, z-scored heat map of phosphosites that are upregulated upon polyamine deprivation (SAM486A 1 µM + DFMO 50 µM, 48 h) and their reversibility following supplementation with exogenous polyamines (putrescine, spermidine, and spermine; 10 µM for 48 h). **c**, Schematic representation of the conservation across species of the main altered phosphosites upon PA deprivation in SF3A1, SF3A3 and SF3B2. Arrows highlight the position of phosphorylated serines (S) or threonines (T) altered upon PA deprivation. **d**, Schematic model representing the impact of PA deprivation in the phosphorylation of SFs and the subsequent perturbation on pre-mRNAs alternative splicing. Created in BioRender. Biorender1, A. (2025) https://BioRender.com/zitthjc. **e**, Phosphorylation levels of SF3A3 at Ser365, Ser367, Ser369 and Thr475 in DU145 cells upon polyamine deprivation (SAM486A 1 µM + DFMO 50 µM, 48 h) and following supplementation with exogenous polyamines (putrescine, spermidine, and spermine; 10 µM for 48 h). Abbreviations: S: SAM486A, D: DFMO, PA: polyamines, S:Serine, T:threonine. Statistics: Two-tailed Mann-Whitney U-test is applied in (**a**). p: p-value.

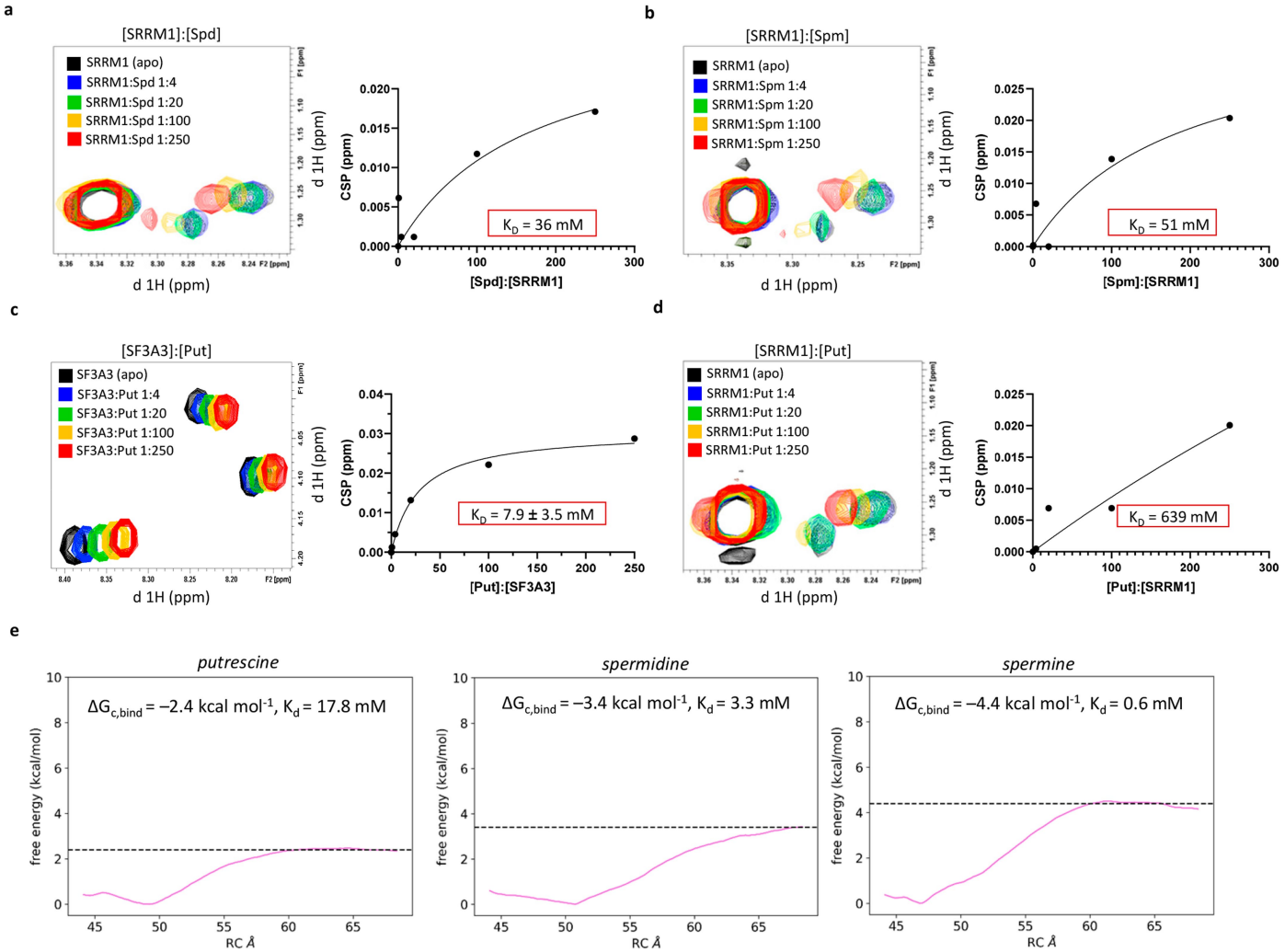

Extended Data Fig. 6 | Polyamines establish highly dynamic interactions with the acidic phosphorylation motif of U2 snRNP SF3A3 member. **a**,**b**, Selected region of the overlaid ^{1}H-^{1}H-TOCSY NMR spectra of the SRRM1 fragment in the absence (black) or presence (from blue to red) of increasing amounts of spermidine (**a**) or spermine (**b**) and their quantification. One spectrum recorded along the titration is not shown for the sake of clarity. The arrow indicates the shift in the signal that was used to derive the affinity of the interaction. Chemical shift perturbation of the signal in the spectra along the titration is also shown for spermidine (**a**) and spermine (**b**). The line is the fitting to a 1:1 binding model and the constant dissociation is indicated with the standard error. **c**,**d**, Selected region of the overlaid ^{1}H-^{1}H-TOCSY NMR spectra of SF3A3 peptide (**c**) and the SRRM1 fragment (as a negative control) (**d**) in the absence (black) or presence (from blue to red) of increasing amounts of putrescine and their quantification. One spectrum recorded along the titration is not shown for the sake of clarity. Chemical shift perturbation of the signal in the spectra along the titration is also shown for putrescine. The line is the fitting to a 1:1 binding model and the constant dissociation is indicated with the standard error. **e**, Initial geometries and potential of mean force (PMF) profiles for the binding free energy calculations of putrescine (left), spermidine (middle) or spermine (right) with SF3A3 by umbrella sampling simulations. Abbreviations: ppm: parts per million, CSP: Chemical shift perturbation, Kd: Dissociation constant.

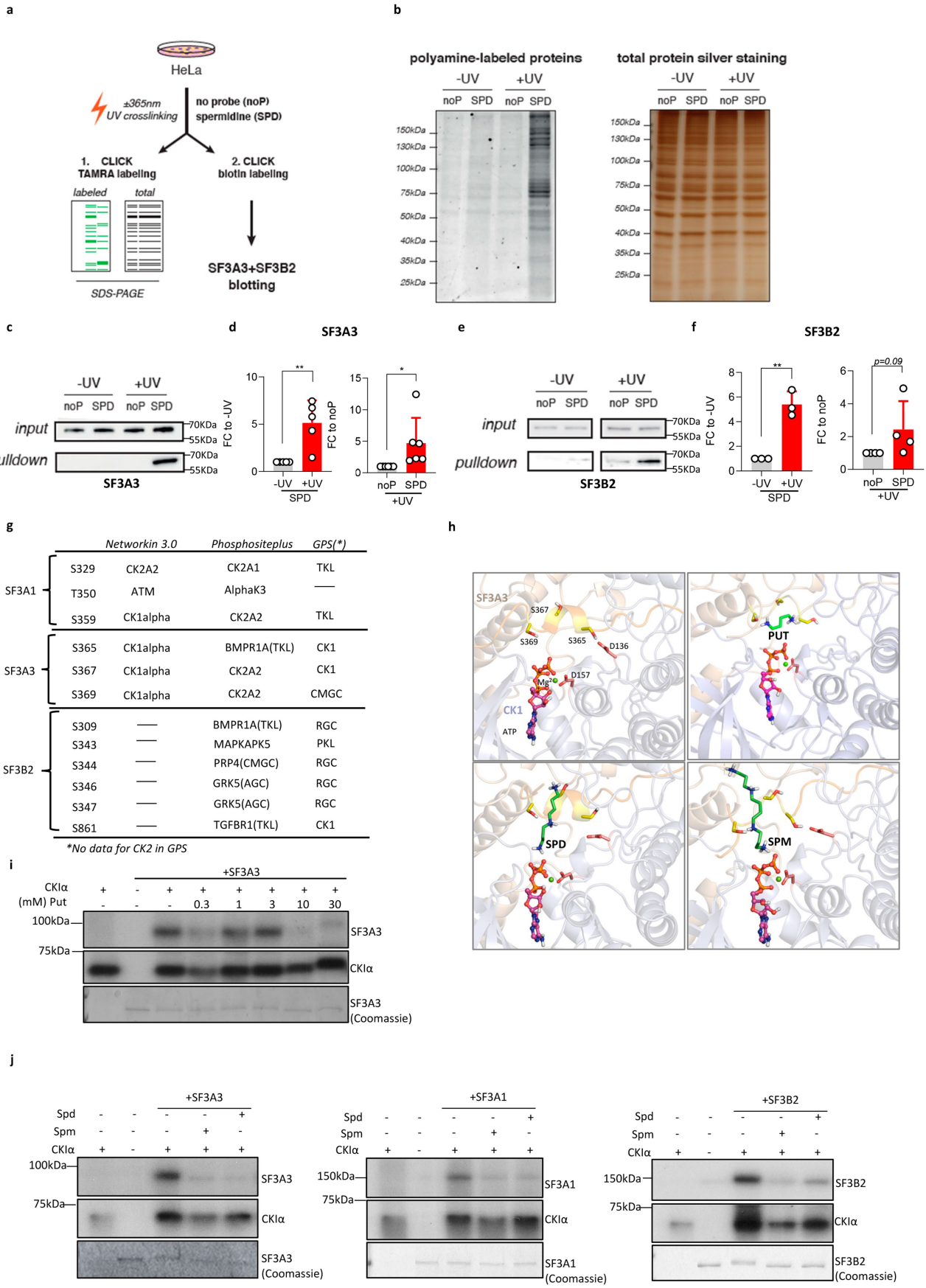

Extended Data Fig. 7 | See next page for caption.

Extended Data Fig. 7 | Polyamines bind acidic phosphorylation motifs of U2 snRNP SF3 subcomplex members preventing the action of kinases. **a**, Schematic representation of experimental design. **b**, SDS-PAGE of TAMRA-labelled proteins (left) and silver staining of total protein (right) in HeLa cells incubated with or without the spermidine photoaffinity probe and irradiated for crosslinking (10 min). **c**, **d**, Western blot using SF3A3 antibody (**c**) and corresponding quantification (**d**) of biotin-labelled proteins pulled down with streptavidin beads. **e**, **f**, Western blot using SF3B2 antibody (**e**) and corresponding quantification (**f**) of biotin-labelled proteins pulled down with streptavidin beads. **g**, Summary table of a kinase prediction with three different webtools (*Networkin 3.0, Phosphositeplus (2023)* and *GPS 6.0*) of the main altered phosphosites upon PA deprivation in SF3 complex members (SF3A1, SF3A3, SF3B2). **h**, Left, top: Representation of the ATP-binding site of the SF3A3:CK1 complex, with the C-terminal helix of SF3A3 inserted in the CK1 catalytic domain. Snapshot from a MD simulation (t = 10 ns) of the SF3A3:CK1 complex in the presence of putrescine (in green sticks) (right, top), spermidine (in green sticks) (left, bottom) or spermine (in green sticks) (right, bottom). ATP is shown as magenta balls-and-sticks, Mg^{2+} as a green sphere, and the SF3A3 phosphorylatable positions (Ser365, Ser367, and Ser369) as yellow sticks. Catalytic residues in CK1 (Asp157 and Asp136) are shown as pink sticks. Non-polar hydrogens are omitted for clarity. **i**, Autoradiography of the ^{32}P incorporation in SF3A3 in an in vitro kinase assay in the absence or presence of increasing concentrations of putrescine. **j**, Autoradiography of the ^{32}P incorporation in SF3A3 (left), SF3A1 (middle) and SF3B2 (right) and CK1 in an in vitro kinase assay in the absence or presence of 3 mM of spermidine (Spd) or spermine (Spm). Abbreviations: SPD: Spermidine photoaffinity probe, noP: no probe, UV: Ultraviolet. Statistics: One tailed one-sample t-test is applied in (**d**) and (**f**). *$p < 0.05$, **$p < 0.01$. Error bars: Mean ± S.E.M. n= independent biological replicates (**c**, **d**: 5 SPD, 6 UV; **e**, **f**: 3 SPD, 4 UV; **i**: 2; **j**: 2).

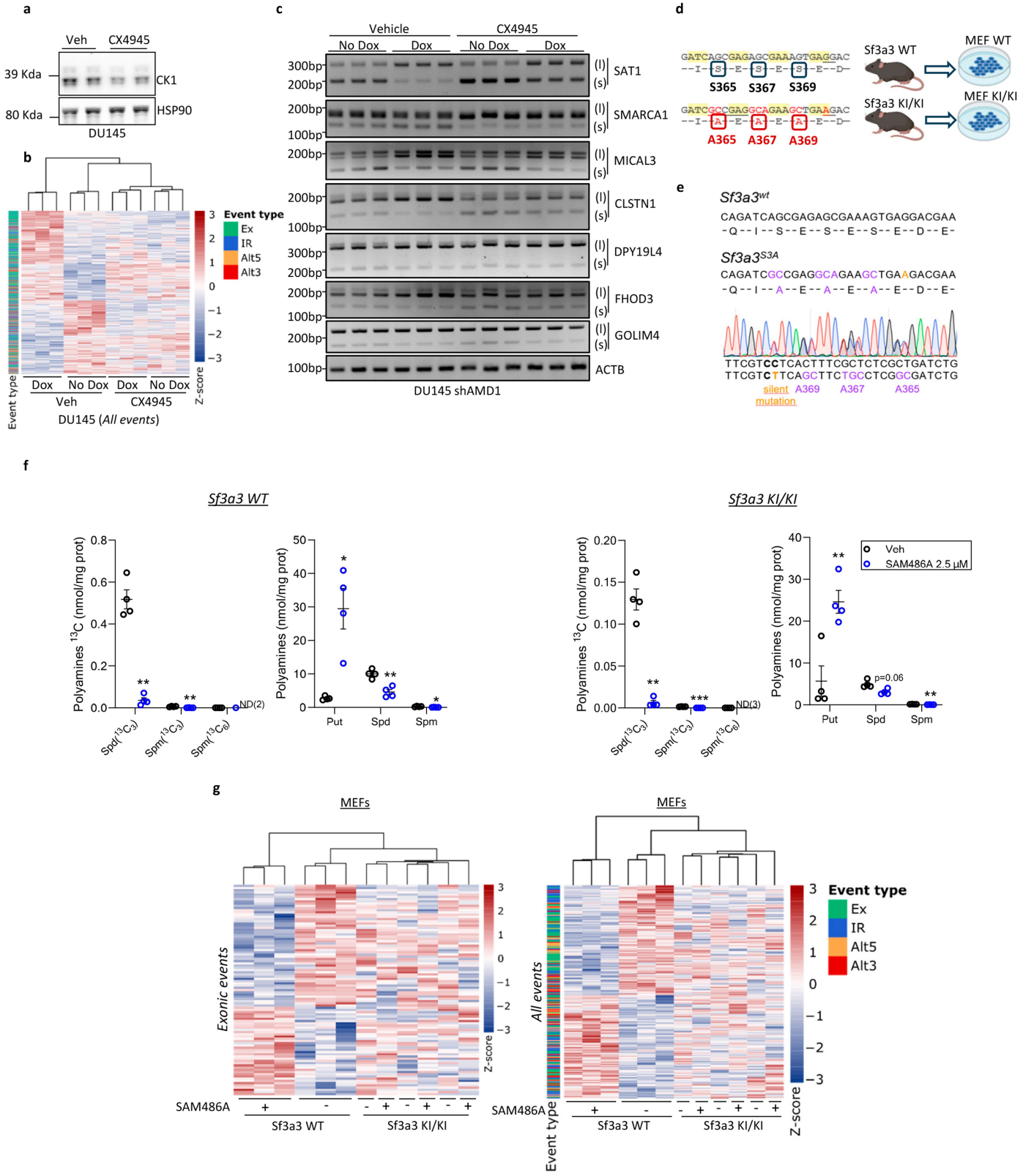

Extended Data Fig. 8 | See next page for caption.

Extended Data Fig. 8 | Casein kinase inhibition or mutation of SF3A3 Ser365/367/369 prevents polyamine deprivation–induced alternative splicing. a, Western blot analysis of CK1 expression in DU145 cells treated with the CK inhibitor CX4945 (10 μM, 48 h). **b**, **c**, z-scored heat map (Abs(ΔPSI) > 10 %, adj-p < 0.1) representation of all the alternative splicing events (**b**), and semi-quantitative PCR gels of selected AS events (**c**) in DU145 sh*AMD1* cells silenced with doxycycline (100 ng/mL, 48 h), with or without CX4945 co-treatment (10 μM, 24 h). **d**, **e**, Schematic representation of the experimental design (https://BioRender.com/1byzvwp) (**d**) and genotyping strategy by sequencing (**e**) of CRISPR-Cas9–generated mice transduced with either wild-type (WT) or mutant *Sf3a3* in which the phosphosites Ser365, Ser367, and Ser369 were replaced by alanine. **f**, **g**, LC-MS metabolomics of total polyamines and [^{13}C]-methionine incorporation (WT, left; KI/KI, right) (**f**), and z-scored heat map representation of exonic events (left) and all the alternative splicing events (right) (**g**) in mouse embryonic fibroblasts (MEFs) treated with or without SAM486A (2.5 μM, 48 h). Abbreviations: Dox: Doxycycline, S: serine; A: alanine; WT: wild type; KI/KI: knock-in; MEF: mouse embryonic fibroblast. ND: non-detectable. Statistics: One-tailed paired t-test was used in (**f**). *p < 0.05, **p < 0.01, ***p < 0.001. Error bars: Mean ± S.E.M. n= independent biological replicates (**a**: 3; **c**: 6; **f**: 4).

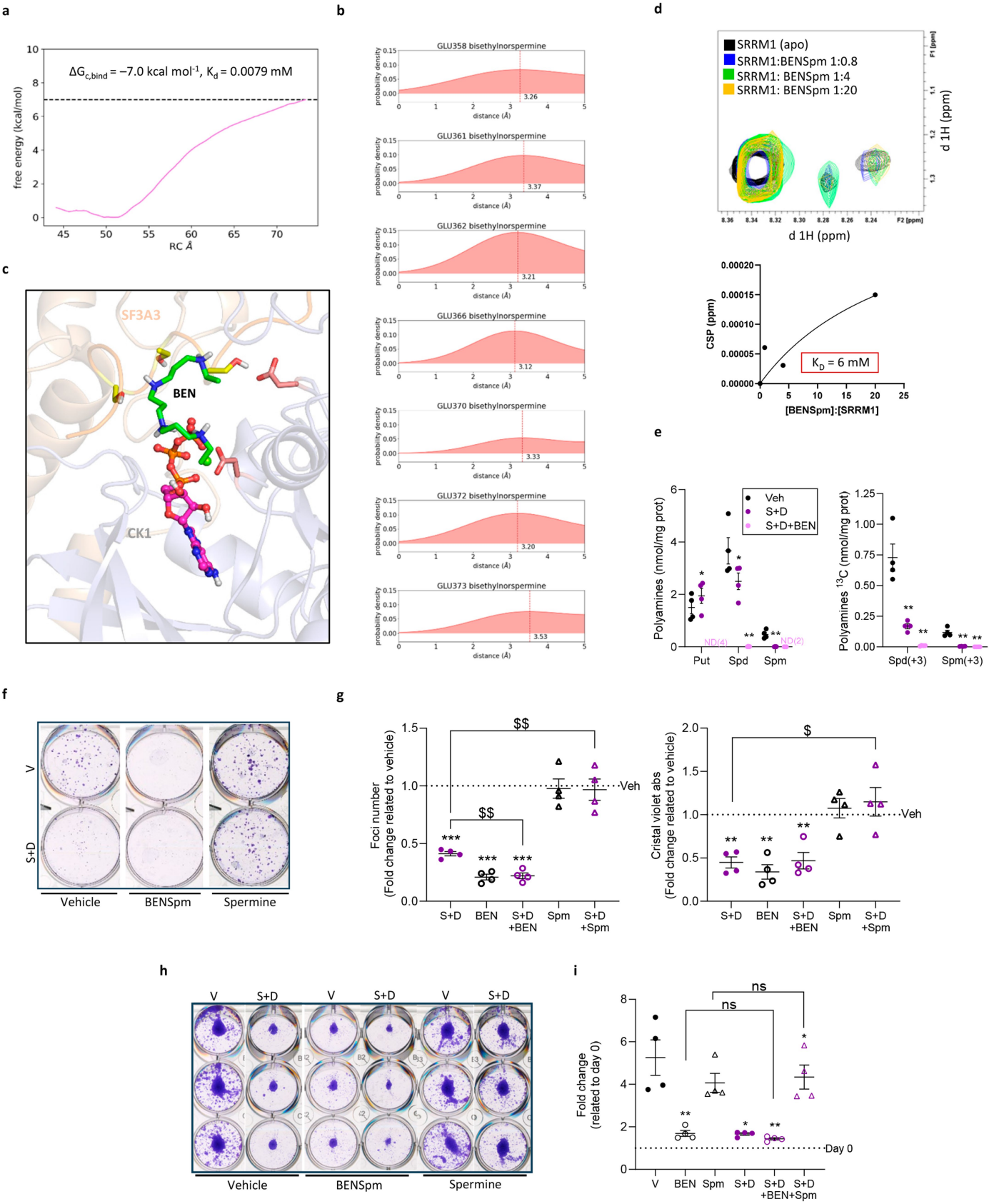

Extended Data Fig. 9 | See next page for caption.

Extended Data Fig. 9 | The polycationic polyamine analogue BENSpm allows the distinction of conventional polyamine activities and metabolic shielding. a, Potential of mean force (PMF) profiles for the binding free energy calculations of BENSpm with SF3A3 by umbrella sampling simulations. **b**, Kernel density estimates of salt bridge distances involving BENSpm and seven selected glutamic residues flanking the phosphorylatable positions Ser365, Ser367, and Ser369. A maximum in the 3—3.6 Å range is indicative of the presence of dynamic salt bridges with BENSpm. **c**, Snapshot from a MD simulation (t = 10 ns) of the SF3A3:CK1 complex in the presence of BENSpm (in green). ATP: magenta balls-and-sticks; Mg^{2+}: green sphere; phosphorylatable residues (Ser365, Ser367, Ser369): yellow sticks; CK1 catalytic residues (Asp157, Asp136): pink sticks. Non-polar hydrogens omitted. **d**, Selected region of the overlaid 1H-1H-TOCSY NMR spectra of SRRM1 fragment (as a negative control) in the absence (black) or presence (from blue to yellow) of increasing amounts of BENSpm (top) and their quantification (bottom). One spectrum recorded along the titration is not shown for the sake of clarity. The line is fitting to a 1:1 binding model and the constant dissociation is indicated with the standard error. **e**, LC-MS quantification of total polyamines (left) and [^{13}C]-methionine incorporation (right) in DU145 cells treated ± SAM486A (1 μM) + DFMO (50 μM) and ± BENSpm (10 μM). **f**–**i**, Foci formation and growth assays in DU145 cells treated with SAM486A (1 μM) + DFMO (50 μM) ± BENSpm (10 μM) or spermine (10 μM). Representative colony formation (**f**); quantification: colony number (left), crystal violet absorbance (right) (**g**); representative growth assay by crystal violet staining (**h**); quantification of growth experiments (**i**). Abbreviations: S: SAM486A, D: DFMO, ppm: parts per million, CSP: chemical shift perturbation. ND: non-detectable. Statistics: One-tailed paired student's t-test for metabolomics (**e**). One-tailed one-sample t-test for quantifications in (**g**,**i**). *p < 0.05, **p < 0.01, ***p < 0.001. Dollar signs: Two-tailed paired t-test comparing S + D vs S + D+BENSpm or S + D+Spm (**g**, **i**). $ p < 0.05, $$ p < 0.01. Error bars: Mean ± S.E.M. n= independent biological replicates (**e**, **f**, **g**, **h**, **i**: 4).

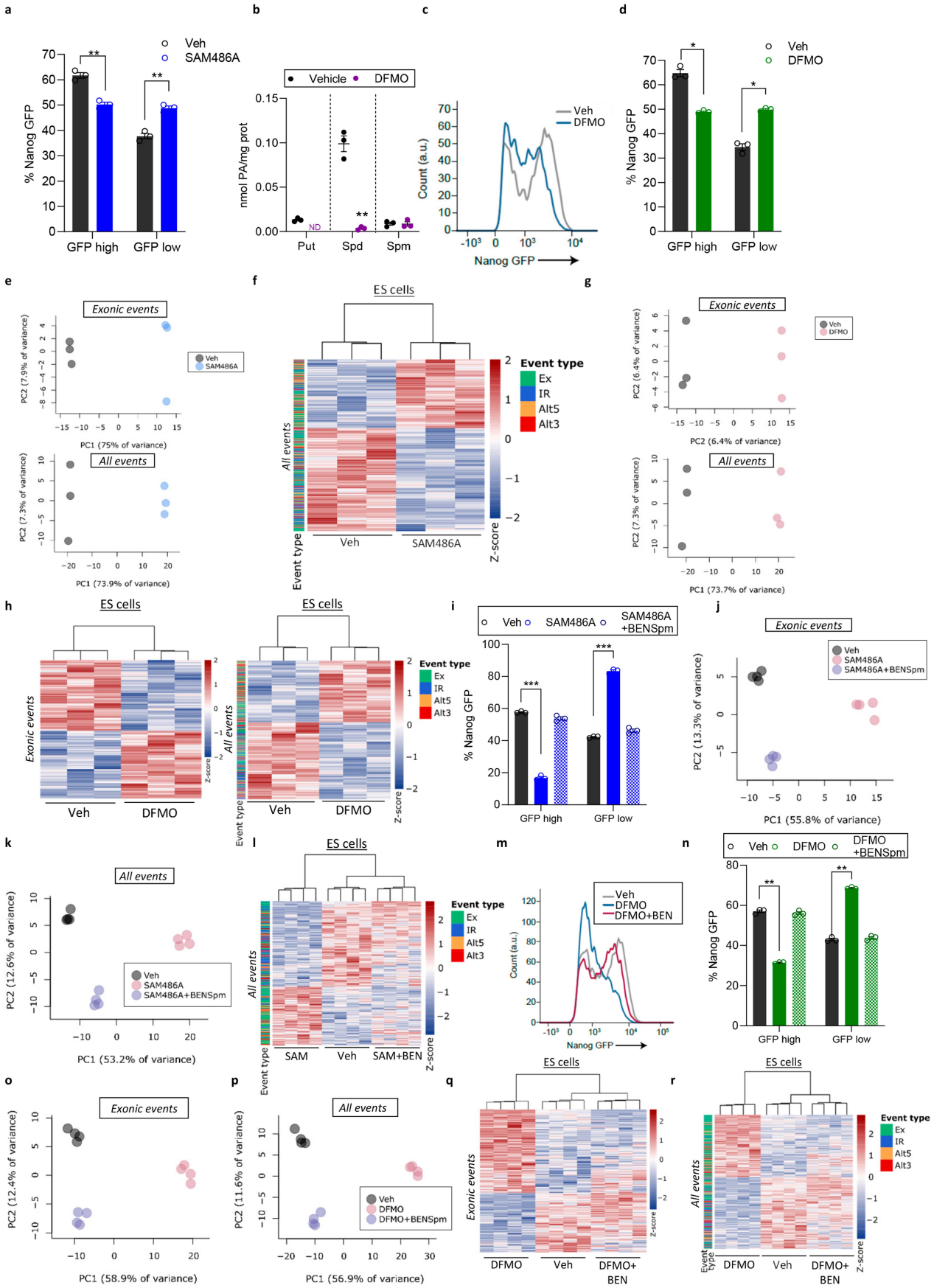

Extended Data Fig. 10 | See next page for caption.

Extended Data Fig. 10 | Regulation of embryonic stem (ES) cell differentiation by polyamine-dependent metabolic shielding. a, Bar plot quantification of the percentage of GFP high and GFP low populations based on FACS analysis of Nanog-GFP expression in ES cells treated with SAM486A (0.5 μM) for 48 h. **b**-**d**, LC-MS quantification of polyamine levels (**b**), representative Nanog-GFP expression measured by flow cytometry (**c**), and bar plot quantification of GFP high and GFP low populations (**d**) in ES cells treated with DFMO (50 μM) for 48 h. **e**,**f**, PCA of RNA-seq based on exonic events (top) and all detected splicing events (bottom) (**e**), and Z-scored heatmap representation of alternative splicing events (all events) (**f**) in ES cells treated with or without SAM486A for 48 h. **g**,**h**, PCA of RNA-seq based on exonic events (top) and all detected splicing events (bottom) (**g**), and z-scored (Abs(ΔPSI) > 10 %, adj-p < 0.1) heat map representation of alternative splicing events exonic, (left) and all events, (right) (**h**) in ES cells treated with or without DFMO for 48 h. **i**-**l**, Bar plot quantification of the percentage of GFP high and GFP low populations based on FACS analysis of Nanog-GFP expression (**i**), PCA of RNA-seq based on exonic events (**j**) and all detected splicing events (**k**), and Z-scored (Abs(ΔPSI) > 10 %, adj-p < 0.1) heatmap representation of alternative splicing events (all events) (**l**) in ES cells treated with SAM486A for 48 h in the presence or absence of BENSpm. **m**-**r**, Representative experiment of Nanog-GFP expression measured by flow cytometry (**m**), bar plot quantification of GFP high and GFP low populations (**n**), PCA of RNA-seq based on exonic events (**o**) and all detected splicing events (**p**) and Z-scored heatmap representation of alternative splicing exonic events (**q**) and all events (**r**) in ES cells treated with or without DFMO for 48 h in the presence or absence of BENSpm. Abbreviations: ES cells: Embrionic stem cells. ND: non-detectable. Statistics: Two-tailed paired student's t-test was used for analysis of GFP bar plots in (**a**, **d**, **i**, **n**) and for metabolomics data in (**b**). *p < 0.05, **p < 0.01, ***p < 0.001. Error bars: Mean ± S.E.M. n= independent biological replicates (**a**, **b**: 3). Flow cytometry analyses in ES cells were performed in two independent biological experiments, and the statistics presented in bar plots were obtained from technical replicates of a representative experiment. (**a**, **c**, **d**, **i**, **m**, **n**:3).

nature portfolio

Corresponding author(s): Arkaitz Carracedo

Last updated by author(s): 18/11/2025

Reporting Summary

Nature Portfolio wishes to improve the reproducibility of the work that we publish. This form provides structure for consistency and transparency in reporting. For further information on Nature Portfolio policies, see our Editorial Policies and the Editorial Policy Checklist.

Statistics

For all statistical analyses, confirm that the following items are present in the figure legend, table legend, main text, or Methods section.

n/a	Confirmed
☐	☒ The exact sample size (*n*) for each experimental group/condition, given as a discrete number and unit of measurement
☐	☒ A statement on whether measurements were taken from distinct samples or whether the same sample was measured repeatedly
☐	☒ The statistical test(s) used AND whether they are one- or two-sided *Only common tests should be described solely by name; describe more complex techniques in the Methods section.*
☒	☐ A description of all covariates tested
☒	☐ A description of any assumptions or corrections, such as tests of normality and adjustment for multiple comparisons
☐	☒ A full description of the statistical parameters including central tendency (e.g. means) or other basic estimates (e.g. regression coefficient) AND variation (e.g. standard deviation) or associated estimates of uncertainty (e.g. confidence intervals)
☐	☒ For null hypothesis testing, the test statistic (e.g. *F*, *t*, *r*) with confidence intervals, effect sizes, degrees of freedom and *P* value noted *Give P values as exact values whenever suitable.*
☒	☐ For Bayesian analysis, information on the choice of priors and Markov chain Monte Carlo settings
☒	☐ For hierarchical and complex designs, identification of the appropriate level for tests and full reporting of outcomes
☒	☐ Estimates of effect sizes (e.g. Cohen's *d*, Pearson's *r*), indicating how they were calculated

Our web collection on statistics for biologists contains articles on many of the points above.

Software and code

Policy information about availability of computer code

Data collection	NA
Data analysis	Software used for molecular modeling data analysis were: Gaussian (16 RevC.01); AlphaFold (2.3.2); GOLD (2023.2.0); Amber (22); AmberTools (22); Python (3.9.19); PyMOL (2.4.0a0). Codes for molecular modeling can be accessed through the Zenodo repository: https://zenodo.org/records/17008960 Codes for the alternative splicing analysis based on RNA-seq data can be accessed through the Zenodo repository: https://doi.org/10.5281/zenodo.17020551 Code for the networks is available in add reference [https://github.com/estepi/SpliceNet – paper https://www.science.org/doi/10.1126/science.adn8105]

For manuscripts utilizing custom algorithms or software that are central to the research but not yet described in published literature, software must be made available to editors and reviewers. We strongly encourage code deposition in a community repository (e.g. GitHub). See the Nature Portfolio guidelines for submitting code & software for further information.

Data

Policy information about availability of data

All manuscripts must include a data availability statement. This statement should provide the following information, where applicable:

- Accession codes, unique identifiers, or web links for publicly available datasets
- A description of any restrictions on data availability
- For clinical datasets or third party data, please ensure that the statement adheres to our policy

The mass spectrometry proteomics data have been deposited to the ProteomeXchange Consortium via the PRIDE partner repository with the dataset identifier PXD046107 (https://proteomecentral.proteomexchange.org/cgi/GetDataset?ID=PXD046107) for DU145 shAMD1 data and reference PXD065659 (https://proteomecentral.proteomexchange.org/cgi/GetDataset?ID=PXD065659) for DU145 and HeLa cells treated with SAM486A+DFMO with and without PA data.
For in vitro data in SKNBE2 cells treated with DFMO, GEO number is GSE301290 and for the in vivo data of TH-MYCN cells injected in mice and treated with DFMO the GEO reference is GSE244378. For the rest of RNaseq data, GEO accession number was identified as GSE255769.

Research involving human participants, their data, or biological material

Policy information about studies with human participants or human data. See also policy information about sex, gender (identity/presentation), and sexual orientation and race, ethnicity and racism.

Reporting on sex and gender	*Use the terms sex (biological attribute) and gender (shaped by social and cultural circumstances) carefully in order to avoid confusing both terms. Indicate if findings apply to only one sex or gender; describe whether sex and gender were considered in study design; whether sex and/or gender was determined based on self-reporting or assigned and methods used.* *Provide in the source data disaggregated sex and gender data, where this information has been collected, and if consent has been obtained for sharing of individual-level data; provide overall numbers in this Reporting Summary. Please state if this information has not been collected.* *Report sex- and gender-based analyses where performed, justify reasons for lack of sex- and gender-based analysis.*
Reporting on race, ethnicity, or other socially relevant groupings	*Please specify the socially constructed or socially relevant categorization variable(s) used in your manuscript and explain why they were used. Please note that such variables should not be used as proxies for other socially constructed/relevant variables (for example, race or ethnicity should not be used as a proxy for socioeconomic status).* *Provide clear definitions of the relevant terms used, how they were provided (by the participants/respondents, the researchers, or third parties), and the method(s) used to classify people into the different categories (e.g. self-report, census or administrative data, social media data, etc.)* *Please provide details about how you controlled for confounding variables in your analyses.*
Population characteristics	*Describe the covariate-relevant population characteristics of the human research participants (e.g. age, genotypic information, past and current diagnosis and treatment categories). If you filled out the behavioural & social sciences study design questions and have nothing to add here, write "See above."*
Recruitment	*Describe how participants were recruited. Outline any potential self-selection bias or other biases that may be present and how these are likely to impact results.*
Ethics oversight	*Identify the organization(s) that approved the study protocol.*

Note that full information on the approval of the study protocol must also be provided in the manuscript.

Field-specific reporting

Please select the one below that is the best fit for your research. If you are not sure, read the appropriate sections before making your selection.

☒ Life sciences ☐ Behavioural & social sciences ☐ Ecological, evolutionary & environmental sciences

For a reference copy of the document with all sections, see nature.com/documents/nr-reporting-summary-flat.pdf

Life sciences study design

All studies must disclose on these points even when the disclosure is negative.

Sample size	For in vitro assays, sample size was determined by establishing a minimum of 3 biological replicates and asssessing data dispersion to increase the number of replicates accordingly. For in vivo assays, we counted on power analysis to establish minimum sample sizes.
Data exclusions	Data exclusions were pre-determined, defining outliers as values exceeding the criteria of mean +/- 2SD.
Replication	Results that were central to the hypothesis were based on a minimum of three biological replicates. In addition, we contemplated data replication through the use of complementary experimental systms for robustness (replications of the results in different cell lines, or through alternative genetic or pharmacological strategies). All attempts to replicate were successful. The majority of partial hypotheses were tested through different experimental or computational strategies for consistency and robustness. These replication also contemplated the inclusion fo technical replicates in each biological replicate to assess data robustness. Key in vitro assays were replicated by individual members of the

research team.

Randomization

In vitro, we did not predetermine the biological samples (cells) that were devoted to a specific perturbations and were assigned randomly to the different regimes. In vivo, we did not pre-assigned mice to specific pharmacological perturbations (in the case of SAM486A treatment) and the assignment of mice to the different experimental groups was random.

Blinding

In the in vitro assays the researchers were not blinded to the experimental perturbations employed. In the in vivo assays the researchers were not blinded to the treatment group. For high throughput analyses (metabolomics, transcriptomics, proteomics) the platform managers and technicians were not blinded to the ID of the samples, but received no information a priori of the expected results when there was a targeted hypothesis.

Behavioural & social sciences study design

All studies must disclose on these points even when the disclosure is negative.

Study description

Briefly describe the study type including whether data are quantitative, qualitative, or mixed-methods (e.g. qualitative cross-sectional, quantitative experimental, mixed-methods case study).

Research sample

State the research sample (e.g. Harvard university undergraduates, villagers in rural India) and provide relevant demographic information (e.g. age, sex) and indicate whether the sample is representative. Provide a rationale for the study sample chosen. For studies involving existing datasets, please describe the dataset and source.

Sampling strategy

Describe the sampling procedure (e.g. random, snowball, stratified, convenience). Describe the statistical methods that were used to predetermine sample size OR if no sample-size calculation was performed, describe how sample sizes were chosen and provide a rationale for why these sample sizes are sufficient. For qualitative data, please indicate whether data saturation was considered, and what criteria were used to decide that no further sampling was needed.

Data collection

Provide details about the data collection procedure, including the instruments or devices used to record the data (e.g. pen and paper, computer, eye tracker, video or audio equipment) whether anyone was present besides the participant(s) and the researcher, and whether the researcher was blind to experimental condition and/or the study hypothesis during data collection.

Timing

Indicate the start and stop dates of data collection. If there is a gap between collection periods, state the dates for each sample cohort.

Data exclusions

If no data were excluded from the analyses, state so OR if data were excluded, provide the exact number of exclusions and the rationale behind them, indicating whether exclusion criteria were pre-established.

Non-participation

State how many participants dropped out/declined participation and the reason(s) given OR provide response rate OR state that no participants dropped out/declined participation.

Randomization

If participants were not allocated into experimental groups, state so OR describe how participants were allocated to groups, and if allocation was not random, describe how covariates were controlled.

Ecological, evolutionary & environmental sciences study design

All studies must disclose on these points even when the disclosure is negative.

Study description

Briefly describe the study. For quantitative data include treatment factors and interactions, design structure (e.g. factorial, nested, hierarchical), nature and number of experimental units and replicates.

Research sample

Describe the research sample (e.g. a group of tagged Passer domesticus, all Stenocereus thurberi within Organ Pipe Cactus National Monument), and provide a rationale for the sample choice. When relevant, describe the organism taxa, source, sex, age range and any manipulations. State what population the sample is meant to represent when applicable. For studies involving existing datasets, describe the data and its source.

Sampling strategy

Note the sampling procedure. Describe the statistical methods that were used to predetermine sample size OR if no sample-size calculation was performed, describe how sample sizes were chosen and provide a rationale for why these sample sizes are sufficient.

Data collection

Describe the data collection procedure, including who recorded the data and how.

Timing and spatial scale

Indicate the start and stop dates of data collection, noting the frequency and periodicity of sampling and providing a rationale for these choices. If there is a gap between collection periods, state the dates for each sample cohort. Specify the spatial scale from which the data are taken

Data exclusions

If no data were excluded from the analyses, state so OR if data were excluded, describe the exclusions and the rationale behind them, indicating whether exclusion criteria were pre-established.

Reproducibility

Describe the measures taken to verify the reproducibility of experimental findings. For each experiment, note whether any attempts to repeat the experiment failed OR state that all attempts to repeat the experiment were successful.

Randomization	*Describe how samples/organisms/participants were allocated into groups. If allocation was not random, describe how covariates were controlled. If this is not relevant to your study, explain why.*
Blinding	*Describe the extent of blinding used during data acquisition and analysis. If blinding was not possible, describe why OR explain why blinding was not relevant to your study.*

Did the study involve field work? ☐ Yes ☒ No

Field work, collection and transport

Field conditions	*Describe the study conditions for field work, providing relevant parameters (e.g. temperature, rainfall).*
Location	*State the location of the sampling or experiment, providing relevant parameters (e.g. latitude and longitude, elevation, water depth).*
Access & import/export	*Describe the efforts you have made to access habitats and to collect and import/export your samples in a responsible manner and in compliance with local, national and international laws, noting any permits that were obtained (give the name of the issuing authority, the date of issue, and any identifying information).*
Disturbance	*Describe any disturbance caused by the study and how it was minimized.*

Reporting for specific materials, systems and methods

We require information from authors about some types of materials, experimental systems and methods used in many studies. Here, indicate whether each material, system or method listed is relevant to your study. If you are not sure if a list item applies to your research, read the appropriate section before selecting a response.

Materials & experimental systems

n/a	Involved in the study
☐	☒ Antibodies
☐	☒ Eukaryotic cell lines
☒	☐ Palaeontology and archaeology
☐	☒ Animals and other organisms
☒	☐ Clinical data
☒	☐ Dual use research of concern
☒	☐ Plants

Methods

n/a	Involved in the study
☒	☐ ChIP-seq
☐	☒ Flow cytometry
☒	☐ MRI-based neuroimaging

Antibodies

Antibodies used	Anti-AMD1 (11052-1-AP, Proteintech; validated through the use of RNAi); anti-ODC1 (17003-1-AP, Proteintech, validated using shRNA); anti-PAOX (18972-1-AP, Proteintech, calidated by company in samples of human stomach tissue); anti-SAT1 (10708-1-AP, Proteintech, validated by company in untreated and DENSPM treated HEK-293 and HeLa cells); anti-SMOX (15052-1-AP, Proteintech, validated by company using extracts of PC-13, A549, HeLa, MCF-7 and PC-3 cells); anti-CK1 (2655, CST, ; validated through the use of RNAi) and anti-HSP90 (4874S, CST, validated by company using extracts of HeLa, NIH/3T3 and COS cells).
Validation	Antibody specificity was verified by the research group or the provider company as indicated for each reference above.

Eukaryotic cell lines

Policy information about cell lines and Sex and Gender in Research

Cell line source(s)	The human prostate carcinoma cell lines used were purchased from Leibniz-Institut DSMZ (Deutsche SammLung von Mikroorganismen und Zellkulturen GmbH), which provided authentication certificate: DU145 (ACC261), PC3 (ACC465), 22RV1 (ACC438) and human benign prostatic hyperplasia (BPH) (ACC143). WPMY-1 prostate stroma fibroblast cell line was purchased from ATCC (CRL-2854). Virus packaging cell line (HEK 293FT; Invitrogen) was kindly provided by Dr. Rosa Barrio and Dr. Jim Sutherland. Human breast cancer cell lines were purchased from DMSZ: MCF7 (ACC115) and MDA-MB-231 (ACC732). Human melanoma cell line A375 was purchased from ATCC (CRL-1619). Dr. Juan Valcarcel generously provided HeLa cervical carcinoma cell line (purchased from ATCC). SKNBE2 cell line were provided by the Children's Oncology Group Cell Culture Repository (cccells.org) with authentication certificate.
Authentication	DMSZ and ATCC provided authentication certificate of cells. Authentication was performed monitoring STRs in Instituto de Investigaciones Biomédicas Sols-Morreale (IIBM), or with Eurofins for HeLa cells.
Mycoplasma contamination	In all the cases cells tested negative for mycoplasma.

Commonly misidentified lines (See ICLAC register)	No commonly misidentified cell lines were used.

Animals and other research organisms

Policy information about studies involving animals; ARRIVE guidelines recommended for reporting animal research, and Sex and Gender in Research

Laboratory animals	All the experimental procedures involving the use of mice were carried out following the ethical guidelines established by the Biosafety and Animal Welfare Committee at CICbioGUNE. Moreover, the procedures employed were performed in concordance with the recommendations stablished by the AAALAC. Mice in a mixed background were housed under controlled environmental conditions, such as gggggtime-controlled lighting on standard 12:12 light: dark cycles, controlled temperature at 22 ± 2ºC and 30-50% relative humidity. Mice were fed regular chow diet ad libitum and fasted for 6 h prior to tissue harvest (9 am-3 pm) to prevent metabolic alterations due to immediate food intake. At experimental endpoint, all mice were sacrificed by CO2 inhalation followed by cervical dislocation. For the SAM486A in vivo study, male mice from a mixed C57BL6/J,129SV,FVB background were used at an age window of 11-14 weeks.
Wild animals	No
Reporting on sex	For the in vivo SAM486A analysis we employed male mice in order to study prostate tissue, which represented the founding tumor type employed in the study.
Field-collected samples	no
Ethics oversight	The study was reviewed, evaluated and approved by the Bioethics and Animal Welfare Committee at CIC bioGUNE, and certified by the corresponding authority (agriculture department, Basque Government. Approval code P-CBG-CBBA-0121).

Note that full information on the approval of the study protocol must also be provided in the manuscript.

Plants

Seed stocks	*Report on the source of all seed stocks or other plant material used. If applicable, state the seed stock centre and catalogue number. If plant specimens were collected from the field, describe the collection location, date and sampling procedures.*
Novel plant genotypes	*Describe the methods by which all novel plant genotypes were produced. This includes those generated by transgenic approaches, gene editing, chemical/radiation-based mutagenesis and hybridization. For transgenic lines, describe the transformation method, the number of independent lines analyzed and the generation upon which experiments were performed. For gene-edited lines, describe the editor used, the endogenous sequence targeted for editing, the targeting guide RNA sequence (if applicable) and how the editor was applied.*
Authentication	*Describe any authentication procedures for each seed stock used or novel genotype generated. Describe any experiments used to assess the effect of a mutation and, where applicable, how potential secondary effects (e.g. second site T-DNA insertions, mosiacism, off-target gene editing) were examined.*

Flow Cytometry

Plots

Confirm that:

☒ The axis labels state the marker and fluorochrome used (e.g. CD4-FITC).

☒ The axis scales are clearly visible. Include numbers along axes only for bottom left plot of group (a 'group' is an analysis of identical markers).

☐ All plots are contour plots with outliers or pseudocolor plots.

☒ A numerical value for number of cells or percentage (with statistics) is provided.

Methodology

Sample preparation	Cells were harvested using trypsin and resuspended in flow cytometry buffer (PBS with 2% FBS, 0.5 mM EDTA, and 0.05% sodium azide) with DAPI. All experiments were analysed on a flow cytometer within 30 minutes of harvest.
Instrument	GFP signal was measured on a BD LSRFortessa flow cytometer.
Software	Data was collected using FACSDiva software v.8.0 (BD Biosciences) and analysed using FlowJo v10.9.0.
Cell population abundance	Clonal cells lines were used for all experiments.

Gating strategy	The gating strategy was initially FSC-A by SSC-A, followed by doublet exclusion using FSC-H and SSC-H, and finally viable cell identification via DAPI exclusion.

☒ Tick this box to confirm that a figure exemplifying the gating strategy is provided in the Supplementary Information.